

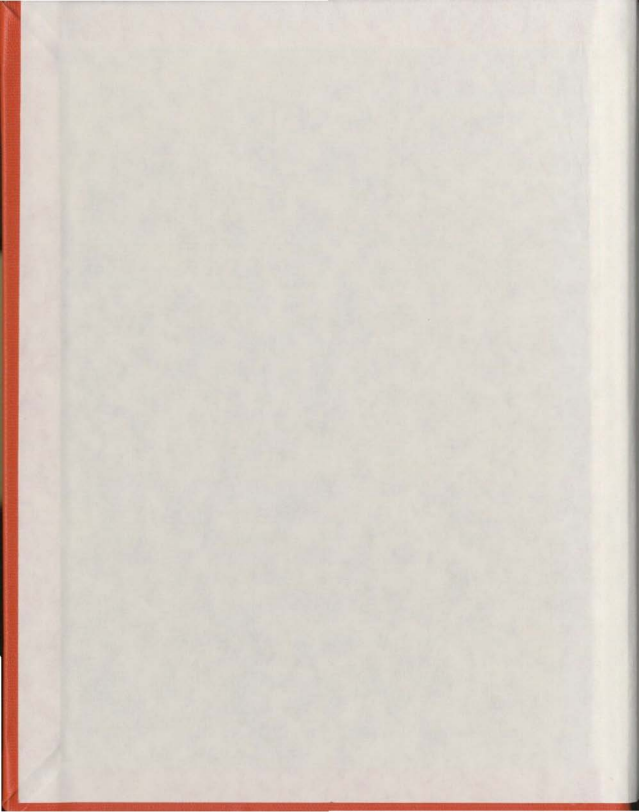
A DIGITAL ACOUSTIC UNDERWATER
COMMUNICATION SYSTEM

CENTRE FOR NEWFOUNDLAND STUDIES

**TOTAL OF 10 PAGES ONLY
MAY BE XEROXED**

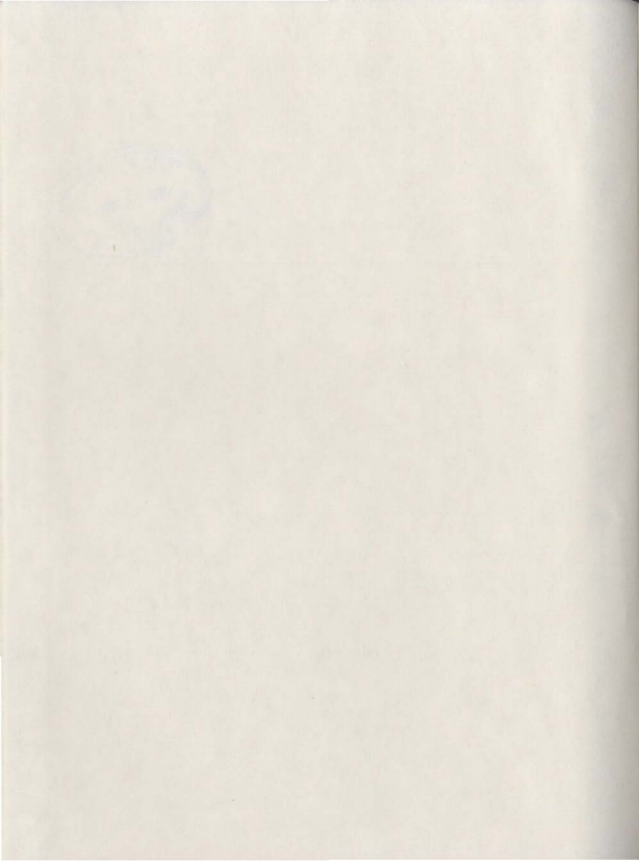
(Without Author's Permission)

EVERETT DWIGHT HOWSE



CO747C





CANADIAN THESES ON MICROFICHE

I.S.B.N.

THESES CANADIENNES SUR MICROFICHE



National Library of Canada
Collections Development Branch

Canadian Theses on
Microfiche Service

Ottawa, Canada
K1A 0N4

Bibliothèque nationale du Canada
Direction du développement des collections

Service des thèses canadiennes
sur microfiche

NOTICE

The quality of this microfiche is heavily dependent upon the quality of the original thesis submitted for microfilming. Every effort has been made to ensure the highest quality of reproduction possible.

If pages are missing, contact the university which granted the degree.

Some pages may have indistinct print especially if the original pages were typed with a poor typewriter ribbon or if the university sent us a poor photocopy.

Previously copyrighted materials (journal articles, published tests, etc.) are not filmed.

Reproduction in full or in part of this film is governed by the Canadian Copyright Act; R.S.C. 1970, c. C-30. Please read the authorization forms which accompany this thesis.

THIS DISSERTATION
HAS BEEN MICROFILMED
EXACTLY AS RECEIVED

AVIS

La qualité de cette microfiche dépend grandement de la qualité de la thèse soumise au microfilmage. Nous avons tout fait pour assurer une qualité supérieure de reproduction.

S'il manque des pages, veuillez communiquer avec l'université qui a conféré le grade.

La qualité d'impression de certaines pages peut laisser à désirer, surtout si les pages originales ont été dactylographiées à l'aide d'un ruban usé ou si l'université nous a fait parvenir une photocopie de mauvaise qualité.

Les documents qui font déjà l'objet d'un droit d'auteur (articles de revue, examens publiés, etc.) ne sont pas microfilmés.

La reproduction, même partielle, de ce microfilm est soumise à la Loi canadienne sur le droit d'auteur, SRC 1970, c. C-30. Veuillez prendre connaissance des formules d'autorisation qui accompagnent cette thèse.

LA THÈSE A ÉTÉ
MICROFILMÉE TELLE QUE
NOUS L'AVONS REÇUE

A DIGITAL ACOUSTIC
UNDERWATER COMMUNICATION
SYSTEM

by



Everett Dwight Howse

A thesis submitted in partial fulfillment
of the requirement for the degree of
Master of Engineering

Faculty of Engineering
Memorial University of Newfoundland
September, 1981

St. John's

Newfoundland

A DIGITAL ACOUSTIC
UNDERWATER COMMUNICATION
SYSTEM

by

Everett Dwight Howse, B. Eng.

Faculty of Engineering
Memorial University of Newfoundland
September, 1981

St. John's

Newfoundland

ABSTRACT

There is a need for an underwater communication system capable of reliable data transmission at rates in excess of 10^3 bps. Such a system would have applications in controlling unmanned tetherless submarines or in transmission of slow-scan television pictures through the ocean. The main hinderance to the development of reliable data transmission through water, using acoustic propagation is the multipath interference caused by reflection and refraction in the ocean channel. The effects of multipath may be suppressed using a swept carrier modulation technique.

A prototype swept carrier system using a ramp type of sweep has been designed and built. This system is designed to provide a bandpass channel of reduced multipath which may be used for either analog or digital transmission. The prototype is designed to transmit a 2 kHz message through the ocean by amplitude modulating a swept carrier. Laboratory test using a carrier which is swept from 20 kHz to 40 kHz with a 500 ms repetition rate indicate that this type of system is capable of suppressing the multipath effects. Tests conducted at sea identified a need for modifications which are required before the prototype can be developed into a full-scale underwater acoustic communication system.

ACKNOWLEDGEMENTS

There are many people whose help has been greatly appreciated through the various stages of this thesis.

Thanks are extended to Dr. Adam Zielinski for his moral and technical support as supervisor.

The financial support which C-CORE provided through its fellowship program is gratefully acknowledged.

Thanks to Wally Jacobs and the crews of the "Elsie G" and the "Karl and Jackie" for their assistance during sea trials also to Technical Services for their help in building a prototype system.

Finally, thanks to Mrs. Doris Rowe for her patience in typing this thesis.

TABLE OF CONTENTS

	Page
ABSTRACT	iii
ACKNOWLEDGEMENTS	iv.
LIST OF TABLES	viii
LIST OF FIGURES	ix
LIST OF SYMBOLS	xiii
CHAPTER	
I. INTRODUCTION	
1.1. Need for an Underwater Communication System	1
1.2. Acoustic versus Electromagnetic Propagation	2
1.3. Scope of this Thesis	4
II. UNDERWATER ACOUSTIC COMMUNICATION	
2.1. Introduction	7
2.2. Attenuation	7
2.2.1. Absorption Losses	7
2.2.2. Spreading Losses	9
2.3. Noise	12
2.4. Multipath and its Effects	14
2.4.1. Reflection and Refraction as Causes of Multipath	15
2.4.2. Multipath Determination Using a Ray Trace Program	20

III.	METHODS USED TO SUPPRESS MULTIPATH	
3.1.	Introduction	29
3.2.	Transducer Directivity	29
3.3.	Burst Mode Communication	32
3.4.	Frequency - Hopping	34
3.5.	Swept-Carrier Communication	34
IV.	DEVELOPMENT OF A SWEPT-CARRIER SYSTEM	
4.1.	Design Considerations	38
4.1.1.	Choice of Sweeping Waveform	38
4.1.2.	Carrier Frequency Selection	42
4.1.3.	Ambient Noise Considerations	46
4.1.4.	Multipath Noise Considerations	49
4.1.5.	Choice of Modulation Technique	58
4.2.	Prototype Design	59
4.2.1.	Introduction	59
4.2.2.	Swept-Carrier Modulator Board	61
4.2.3.	Data Generator Board	61
4.2.4.	The Receiver	65
4.2.5.	Transducer Selection	74
4.2.6.	Prototype Housing	75
4.3.	Prototype Testing	76
4.3.1.	Laboratory Testing	78
4.3.2.	Sea Trials	84
V.	CONCLUSIONS	95
BIBLIOGRAPHY AND LIST OF REFERENCES		97

APPENDICES

A. Time Spread due to Frequency-dependent Absorption	103
B. Ray Trace Program	109
C. Eigenray Response Program	115
D. Schematic Diagrams	121
E. Transducer Frequency Response	126

LIST OF TABLES

- Table 4.1 Transmission Requirements for Selected
Analog Signals
- Table 4.2 Catalogue of Multiplier Output Frequencies
and their Separations from the Intermediate
Frequency
- Table 4.3 Multipath Suppression Obtained for Various
Separations between two 500 ms Ramps

LIST OF FIGURES

- Figure 1.1 Electromagnetic Propagation Attenuation
in Clear Sea Water
- Figure 1.2 Acoustic Propagation Attenuation in
Sea Water and Distilled Water
- Figure 1.3 Maximum Theoretical Data Transmission Rate
Through the Ocean
- Figure 2.1 Acoustic Absorption Coefficient in
Sea Water
- Figure 2.2 Average Ambient Noise Spectra in Deep Water
- Figure 2.3 Envelope Fluctuations of a 40-kHz
Tone due to Multipath
- Figure 2.4 Boundary Acoustic Reflection Model
- Figure 2.5 Ray Bending in a Medium Horizontally
Stratified by Different Characteristic
Velocities
- Figure 2.6 Typical Ray Trace Program Output Plot
- Figure 2.7 Spreading Loss Model for Ray Trace Program
- Figure 2.8 Typical Eigenray Response Program Plot
- Figure 2.9 Eigenrays of Fig. 2.8 using Ray-Trace
Program
- Figure 3.1a Eigenray Response for 60° Beamwidth
Transducer

- Figure 3.1b Eigenray Response for 10^0 Beamwidth
Transducer
- Figure 3.2 Burst Mode Communication Method
- Figure 3.3 Frequency-Hopping Communication Method
- Figure 3.4 Swept Carrier Modulation Technique
- Figure 4.1 * Impulse Response Model of the Ocean
Channel due to Multipath
- Figure 4.2 Multipath Interference of a
Swept-Carrier with Sinusoidal Sweep
- Figure 4.3 Multipath Interference of a Swept-Carrier
with Ramp Sweep
- Figure 4.4 Plot of Optimum Carrier Frequency Versus
Range
- Figure 4.5 Expected Probability of Error versus
System Parameter for ASK and FSK
- Figure 4.6 Multipaths of a Communication
System in an Ocean of constant velocity.
- Figure 4.7 a-f. Comparisons of Multipath Interference
and Possible Improvement for Various
Conditions
- Figure 4.8 Ocean Configuration for Prototype System
- Figure 4.9 Prototype Transmitter showing Hydrophone,
Circuitry, Tape Recorder and Batteries

- Figure 4.10 Block Diagram of Swept-Carrier Modulator Board
- Figure 4.11 Block Diagram of Pseudo-random Data Generator Board
- Figure 4.12 Block Diagram of Receiver
- Figure 4.13 Block Diagram of Real Multiplier
- Figure 4.14 Diagram of Receiver Synchronization Logic
- Figure 4.15 Transmitter Mounted in Tripod on Gimbal
- Figure 4.16 Receiving System, Hydrophone, Cable and Onboard Circuitry
- Figure 4.17 Laboratory Test Set-up
- Figure 4.18 Frequency Response of Swept Carrier Message
- Figure 4.19 Block Diagram of Multipath Simulator
- Figure 4.20 Sea Trial Test Scenario
- Figure 4.21 Sea Trial Multipath Condition
- Figure 4.22 Amplitude Fluctuation of constant 35 kHz tone due to Multipath
- Figure 4.23 Amplitude Fluctuation of Swept-Carrier due to Multipath and Transducer Response
- Figure 4.24 Spectral Component of AGC Effect for Constant Carrier

- Figure 4.25 Spectral Component of AGG Effect for
Swept-Carrier
- Figure A.1 Block Diagram of Ocean Transfer
Function
- Figure A.2a-c Impulse Time Spread due
to Ocean Transfer Function
- Figure B.1 Flowchart for Ray Trace Program
- Figure C.1 Flowchart for Eigenray Response Program
- Figure D.1a-e Circuit Schematics
- Figure E.1 Transducer Transmitting Response
- Figure E.2 Measured Transducer Receiving Response

LIST OF SYMBOLS

A	- attenuation from source to receiver in dB
A_s	- transmission loss due to spherical spreading in dB
AGC	- automatic gain control
AM	- amplitude modulation
ASK	- amplitude shift keying
B.	- message bandwidth in Hz
B_s	- signal bandwidth in Hz
C	- sound velocity in m/s
$C_{x,y,z}$	- coordinate dependent sound velocity in m/s
d	- distance between transmitter and receiver in m
DMR	- direct to multipath power ratio in dB
DSBSC	- double sideband suppressed carrier
f	- frequency in Hz
f_c	- carrier frequency in Hz
$f_c(t)$	- instantaneous carrier frequency in Hz
f_H	- maximum carrier frequency in Hz
f_{IF}	- intermediate frequency in Hz
f_L	- minimum carrier frequency in Hz
f_{LO}	- local oscillator frequency in Hz
$f_{LO}(t)$	- instantaneous local oscillator frequency in Hz
f_{opt}	- optimum carrier frequency in Hz
f_{rb}	- relaxation frequency of boric acid in kHz

- f_{rm} - relaxation frequency of magnesium sulphate
in kHz.
- FM - frequency modulation
- FSK - frequency shift keying
- h - RMS wave height measured crest to trough
in m
- $H(f)$ - transfer function
- I - improvement obtained by multipath suppression
in dB
- k - carrier sweep rate in Hz/s
- L_B - bottom reflection loss in dB
- L_s - surface reflection loss in dB
- m - number of multipaths suppressed
- n - number of surface reflections
- N - in-band, in-beam noise in dB re 1 μ Pa
- p - acoustic pressure
- P - system parameter in dB
- $P_{1,2,\dots,n}$ - intensity of n^{th} multipath in dB re 1 μ Pa
- P_D - intensity of direct path in dB re 1 μ Pa
- P_E - probability of error
- P_t - transmitter pressure level in dB re 1 μ Pa at 1m
- PM - phase modulation
- r - data rate in bit/sec
- R - Rayleigh parameter
- s - salinity in ppt.
- S_C - carrier sweep range in Hz

- SNR - signal-to-noise ratio in dB
- SSB - single sideband
- t - time in s
- t_o - arrival time of direct path in s
- $t_{1,2..n}$ - arrival time of n^{th} multipath in s
- t_m - impulse response decay time in s
- T - water temperature in $^{\circ}\text{C}$
- UART - universal asynchronous receiver/transmitter
- v - voltage in volts
- W - percentage of words with parity errors
- y - horizontal distance between source and receiver
in m
- z - depth in m
- a - absorption coefficient in dB/km
- Δh - vertical distance between rays at the receiver
in m
- $\Delta \theta$ - angle between rays at the source in deg.
- η - grazing angle in deg.
- λ - acoustic wavelength in m
- $\phi(f)$ - phase response

CHAPTER I

INTRODUCTION

1.1. Need for an Underwater Communication System

Since his earliest beginnings, man has been striving unceasingly to expand his conception of the world around him. In recent times, this quest for knowledge has led man into explorations of both the frontiers of space and of the oceans. In order to relay information in either of these domains, it is essential that reliable communications systems be developed to operate in these environments. This thesis will be directed toward the development of a communication system for use in the ocean.

The need to transmit data through the ocean at rates of $10^3 - 10^4$ bps is demanded in a variety of applications. With the development of a communication system of this capability, unmanned, tetherless submarines could be controlled from the surface [7], [20]. These submarines could be used for explorations in situations which may be dangerous to man either due to environmental conditions such as great depth or due to military activity.

This data rate is also sufficient for slow-scan television transmission of pictures from the ocean depths to the surface, which could be used, for example, in checking for cracks in the piles of an oil rig or studying the ocean floor composition.

In other situations, it may be necessary to transmit large blocks of data gathered at a bottom unit over a long period of time to an observer at the surface. This situation might occur in a study of temperature or salinity changes or seismic activity at the ocean floor.

Voice communication between untethered divers working in the same area or as a back-up to a cable link are further applications of an underwater communication system.

While in some instances it may be feasible to transmit data through an umbilical cable, or even to store data for later retrieval of the instrumentation, this is not always practical, particularly at great depths. These situations provide the need for a reliable underwater communication system.

1.2. Acoustic versus Electromagnetic Propagation

Although the distances involved in an underwater communication system are small, compared to space communication, it suffers from some unique problems which make the development of a communication system difficult. Long-distance communication through air, or space using electromagnetic propagation, such as, in radio is well established. An electromagnetic carrier, however, is not suitable for transmission over long distances underwater. As can be seen from the diagram of Figure 1.1, [9] the losses involved in electromagnetic propagation can be quite high except in the band of light frequencies. Even at these frequencies though, the attenuation is high if the water is not clear.

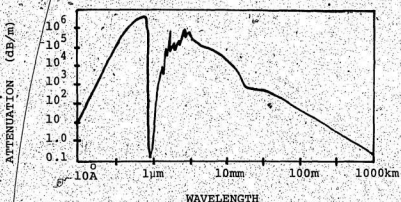


Figure 1.1 Electromagnetic Propagation
Attenuation in Clear Sea Water [9]

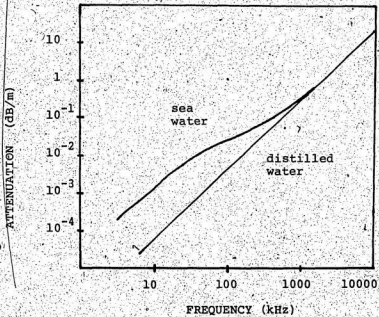


Figure 1.2 Acoustic Propagation Attenuation in
Sea Water and Distilled Water [27]

An alternative to electromagnetic propagation is to use acoustic energy as the means of transmitting information. This idea is neither new, nor original to man - whales and porpoises have been using underwater sound as communication aids for ages. The losses associated with the transmission of acoustic energy through water are much smaller than those of electromagnetic energy. Figure 1.2 [27] shows that, for frequencies less than 50 kHz, the acoustic attenuation coefficient is less than 20dB/km. According to a study by Anderson [11] "for distances in excess of 300 m, acoustic transmission channels in the ocean offer bandwidths four or five orders of magnitude broader than those associated with electromagnetic propagation". For this reason, the author has chosen to use acoustic propagation in the development of an underwater communication system.

1.3 Scope of this Thesis

The bandwidth available using acoustic propagation can theoretically allow transmission rates from 500 bps at 10 km to 10^4 bps for 1 km and higher as the distance decreases, as seen in Figure 1.3 from Marsh [17]. This data rate is severely lowered, however, by random signal fading [17]. This fading is caused by the varying multipath conditions which result from reflections and refractions of an acoustic wave in the ocean channel.

This thesis presents background information relating to

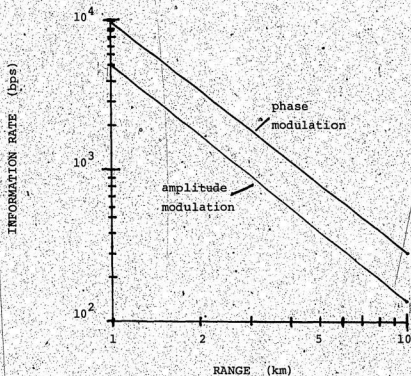


Figure 1.3 Maximum Theoretical Data Transmission Rate Through the Ocean [5]

underwater acoustic propagation with particular emphasis on the sources of multipath and its estimation. Various methods of suppressing multipath are discussed and the development of a digital or analog swept carrier system is described. This prototype system has been tested in the laboratory and the results of these tests show its ability to suppress the multipath effects.

medium, and that this loss should increase with frequency.

At frequencies below about 1 MHz, there is another mechanism which introduces absorption losses to an acoustic wave propagating in seawater. It has been found that attenuation in seawater can be thirty times that of fresh water due to the relaxation of magnesium sulphate molecules dissolved in the water [27]. The relaxation frequency of the magnesium sulphate varies with temperature according to the equation given by Urićk [27].

$$f_{rm} = 21.9 \times 10^6 - 1520/(T + 273) \quad (2.1)$$

where: f_{rm} = the relaxation frequency of magnesium sulphate in kHz

T = water temperature in $^{\circ}\text{C}$

This relaxation frequency increases from 59 kHz to 210 kHz as the water temperature varies from 0°C to 30°C . An acoustic wave with a frequency near the relaxation frequency will undergo significant energy loss due to the concentration of magnesium sulphate in the water.

Further absorption at frequencies below 10 kHz is believed to be due to relaxation of boric acid [6]. The relaxation frequency for boric acid is described according to Clay [6] by the equation:

$$f_{rb} = 0.9 (1.5) T/18 \quad (2.2)$$

where: f_{rb} = the relaxation frequency of boric acid in kHz

T = water temperature in $^{\circ}\text{C}$

This equation sets the relaxation frequency of boric acid around 1 kHz, again depending on temperature.

The combined result of these effects gives rise to a frequency dependent absorption coefficient at 4°C modified from Urick [27]:

$$\alpha' = 1.09 \left| \frac{0.1f^2}{1+f^2} + \frac{40f^2}{4100+f^2} + 2.75 \times 10^{-4} f^2 \right| \quad (2.3)$$

where: α' = absorption coefficient in dB/km

f = frequency in kHz

The absorption versus frequency curves for different ranges have been plotted using this equation in Figure 2.1 clearly indicated is the increase in absorption losses with both frequency and distance. The frequency-dependent change in amplitude due to absorption introduces a small time smear in the impulse response of the ocean which may be found using the Fourier transform. This effect is further explored in Appendix A.

Since the attenuation due to absorption is both frequency and range dependent, the designer must optimize between the desired range of the communication system and the bandwidth available, for a given power input-level.

2.2.2. Spreading Loss

While spreading losses do not represent actual energy gain to the medium, as do absorption losses, they do account for

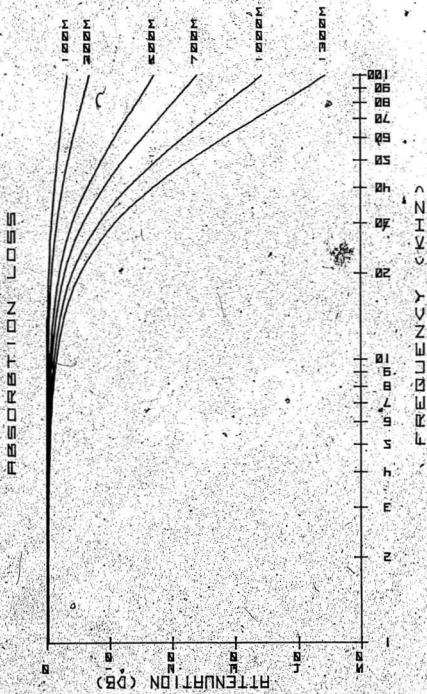


Figure 2.1 Acoustic Absorption Coefficient in Sea Water

an attenuation between the transmitted and received signals. This attenuation arises from the fact that the transmitter generates a finite amount of power over a finite area which in turn gives an energy density at the transmitter. While this energy is propagating toward the receiver, the total energy is spread over an increasing area which results in a decreasing energy density. Since the receiver has only a finite area, it responds to the energy density and hence, there is an apparent loss in the received energy.

In the absence of other means of predicting the spreading of an acoustic wave, spherical spreading may be assumed. In this case, the energy spreads over the surface of a sphere with radius equal to the distance between transmitter and receiver. Since the surface area of a sphere is proportional to the square of the radius, the loss due to spherical spreading may be calculated as:

$$A_s = 20 \log (d) \quad (2.4)$$

where: A_s = transmission loss due to spherical spreading in dB

d = distance between transmitter and receiver in meters.

This equation is useful if no data regarding the bending of acoustic waves is available. If the spreading is shown to be non-spherical, it should be remembered that spreading losses

simply account for the ratio between the energy densities at the transmitter and receiver. This knowledge will enable the designer to make a better prediction of the spreading losses when more data on the spreading characteristic is available.

2.3 Noise

As in all communication channels, an underwater acoustic channel has noise associated with it. The ambient noise of the ocean is generated by various means. Wave action at the surface, seismic activity on the bottom, ship traffic and marine life all contribute to the noise level which must be overcome by a communication system.

Due to its sources, the ambient noise level of shallow water is highly variable. Riter [22] says " Unfortunately no generally applicable shallow water noise measurements are available; consequently the designer must rely on special surveys, and past experience to predict the magnitude and frequency dependence of the background noise ". The noise level can be accounted for over the frequency range of interest, by transmitting at a sufficient pressure level for an adequate signal to noise ratio in the worst case conditions.

A typical graph of ambient noise levels for different shipping and sea state parameters versus frequency is shown in Figure 2.2 from Urick [27] based on the findings of Knudsen [12]. These curves indicate the expected deep water noise levels which must be overcome by a sufficient source level.

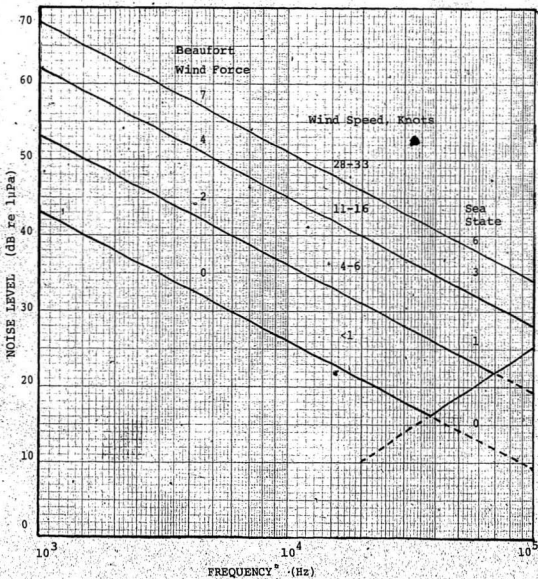


Figure 2.2 Average Ambient Noise Spectra in Deep Water [27]

2.4 Multipath and its Effects

Since the problems of attenuation and noise can be overcome simply, though brutally, by transmitting at a sufficiently high pressure level, at least to the limit of cavitation [27], the main problem associated with underwater acoustic communication is the multipath effect. [1], [19], [30]. Since waves propagating through water do not necessarily travel in straight lines, there may be many paths that an acoustic wave can take between a given transmitter and receiver, hence the term "multipath".

The direction of wave propagation is changed by reflections at the surface or bottom and also by refraction or bending as the wave moves though regions of different characteristic velocities. This means that a particular receiver may at one time receive signals which are bent, reflected from the surface, reflected from the bottom or any combination of these. Since each of these paths have different distances and velocities associated with them, the received signal is a composite of signals sent at different times and is therefore a distorted version of the transmitted signal. The effects of these multipaths include a time smear due to the different travel times of the paths and also a random effect due to surface reflected signals. If the surface is rough, then the ocean wave frequency is impressed on the signal by the Doppler effect, causing a frequency smear. Wave action also causes a randomness in the travel time of surface reflected waves which can cause

constructive or destructive interference at the receiver. The resulting variation in amplitude can be quite pronounced since the travel distance for a 40 kHz signal need only change by 1.8 cm to give complete phase reversal. An experiment conducted on board Memorial University's boat, the "Elsie G" on Conception Bay in June 1980 shows the distortion caused by multipaths. A constant 40 kHz tone was transmitted by an acoustic source directed toward the surface from the ocean floor at 200 m depth. The signal was then received by an omnidirectional hydrophone suspended 2 m below the surface. Figure 2.3. shows the envelope fluctuations of the received tone, lowpass filtered to 12 Hz. The multipath effect is a type of self-noise which must be overcome by an underwater communication system.

2.4.1 Reflection and Refraction as Causes of Multipath

Reflection of acoustic waves at any ocean boundary is one of the mechanisms whereby multipath is generated. Thorough analysis of the reflection process at the surface can only be accomplished statistically, since the surface is a random time-varying boundary due to wave action. Lord and Plemos [15], considered the surface wave height, grazing angle and the acoustic wavelength, in a statistical analysis of the surface reflection phenomenon in the specular direction. This work, however, uses a simplified model of the surface reflection as suggested by Tucker and Gazey [26] whereby incident waves at the surface are reflected at the same angle and in the same plane. Associated with this reflection is a 180° phase shift and a certain power loss. Lytle [16] indicates that for a perfectly smooth surface, this loss would be nearly 0 dB, due to the high

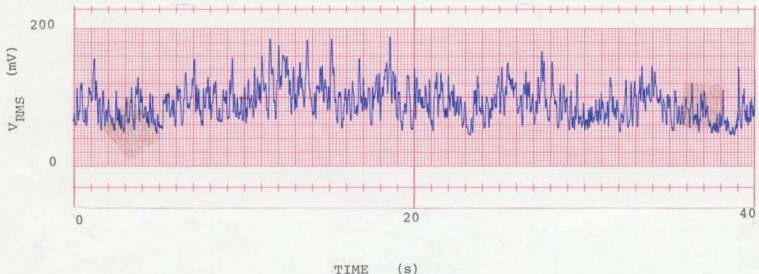


Figure 2.3 Envelope Fluctuations of a 40 kHz
Tone due to Multipath Lowpass Filtered
to 12 Hz.

discontinuity at the air-water boundary. Under normal conditions, however, the loss will be around 3 dB due to the surface roughness. Whether or not the surface may be considered to be smooth depends on the Rayleigh parameter [27]:

$$R = \frac{2\pi h}{\lambda} \sin n \quad (2.5)$$

where: R = Rayleigh parameter

h = RMS wave height measured crest to trough in m

n = grazing angle

λ = acoustic wavelength in m

If $R \ll 1$, then the surface may be considered to be smooth.

Reflection of an acoustic wave at the bottom is considered in the same manner as a surface reflection with reflected angle being equal to the incident angle. Losses at the bottom are higher, however, ranging from 1 dB for a smooth hard bottom to 15 dB for a mud bottom at low grazing angles [16]. The basic reflection model diagram of Figure 2.4 shows the reflection angle equal to the incident angle with associated power loss.

The direction of propagation of an acoustic wave is changed, not only by reflection at the surface or bottom, but also by refraction or bending as the wave travels through the medium. This bending is caused by variations in the characteristic sound velocity for different regions in the medium. The sound velocity was determined by Leroy [14] based on data obtained by Wilson [29] to fit the equation:

$$c = 1449.3 + 4.56 T - .0046 T^2 + (2.6) \\ (1.38 - .01T) (s - 35) + z/61$$

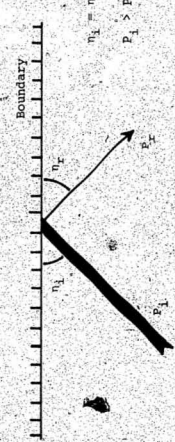


Figure 2.4 Boundary Acoustic Reflection Model

where: c = sound velocity in m/s

T = temperature in $^{\circ}\text{C}$

s = salinity in ppt.

z = depth in m

An acoustic wave moving into a region of different temperature, salinity or depth will change velocity and consequently bend toward the region of lower velocity. The amount of bend may be determined by a second order differential equation known as the wave equation [27]:

$$\frac{\partial^2 p}{\partial t^2} = c_{x,y,z}^2 \left[\frac{\partial^2 p}{\partial x^2} + \frac{\partial^2 p}{\partial y^2} + \frac{\partial^2 p}{\partial z^2} \right] \quad (2.7)$$

where: p = acoustic pressure

t' = time

$c_{x,y,z}$ = coordinate dependent sound velocity

x,y,z = spatial coordinates

While this equation completely defines the propagation of the acoustic waves, it is difficult to solve, particularly at high frequencies. For high frequencies, that is, where the radius of curvature of the wave direction is greater than the wavelength, ray theory gives an easier method of predicting the path bending. The bending of acoustic waves can be found using ray theory in the same manner as it applies to

ray optics, that is, by Snell's Law:

$$\frac{\cos \eta_1}{c_1} = \frac{\cos \eta_2}{c_2}, \quad (2.8)$$

where: η_1, η_2 are the grazing angles for layers 1 & 2
 c_1, c_2 are the characteristic velocities of
 layers 1 & 2

In practical terms, this equation describes the change of direction of a ray as it moves into a region of different characteristic velocity. This effect can be seen in Figure 2.5 which indicates the bending of a ray as it moves through a medium which is divided into layers of different characteristic velocities. As an acoustic wave propagates through the ocean, it is continually moving through regions of different characteristic velocities and hence is continually being refracted.

When the effects of reflection and refraction are taken into account, the paths an acoustic wave will follow may be found and the multipath effects predicted.

2.4.2 Multipath Determination Using a Ray Trace Program

Once the laws governing the reflection and refraction of an acoustic wave have been defined, a computer may be programmed to quickly perform the calculations necessary to predict the wave paths. All that is required to determine the paths an acoustic wave will follow through a particular ocean is

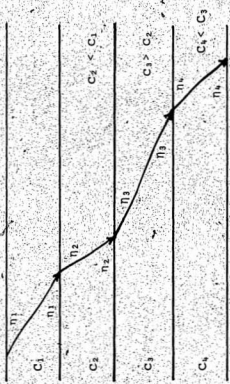


Figure 2.5 Ray Bending in a Medium Horizontally Stratified by Different Characteristic Velocities

the velocity profile of that ocean. This velocity profile may be obtained experimentally for a number of different depths and then, by linear interpolation, the velocity at any depth may be found. If the ocean velocity profile is then used to horizontally stratify the ocean into a large number of layers, each with its own characteristic velocity, the paths an acoustic wave will take from a source may be predicted [28]. These paths can also be plotted using a computer to give a visual representation of the ray paths. A ray trace program has been written for the HP9825 calculator/plotter to aid in the design of an underwater communication system and a typical output plot is shown in Figure 2.6. The velocity profile data used for this plot is based on experimental data obtained by Memorial University during the May 1978 cruise of the Canadian scientific ship "Hudson" on Placentia Bay. This output plot clearly shows the effect of reflection and refraction on the paths an acoustic wave may take through the ocean. A complete program listing and flowchart of the ray-trace program may be found in Appendix B. While this ray-trace program is limited by its inability to consider random ocean wave action or a fluctuating bottom, it does give a reasonable estimate of the acoustic wave paths.

The ray-trace program is also useful in predicting the spreading of an acoustic wave, which, as seen in Figure 2.6, is not always spherical having both convergent and divergent zones. The spreading losses may be calculated since the energy between two rays at the source, remains between

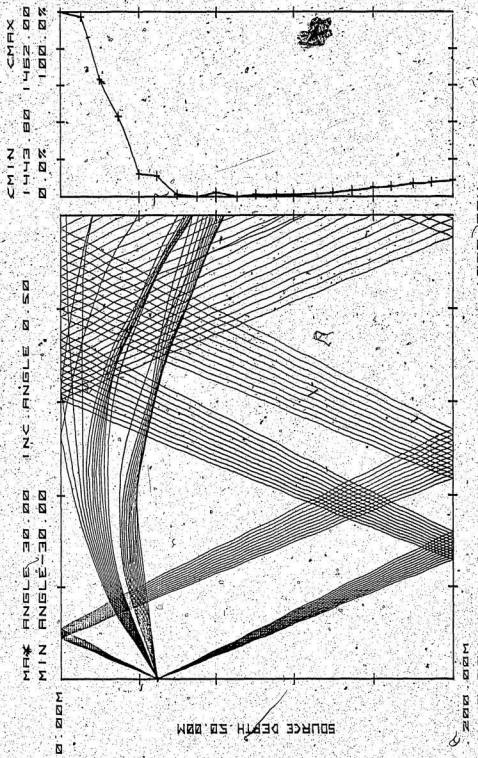


Figure 2.6 Typical Ray Trace Program Output Plot

those two rays, independent of their respective paths. Urick [27] indicates that this loss may be calculated using the equation:

$$A_s = 10 \log \left[\frac{68.53 \text{ yah}}{\Delta\theta} \right] \quad (2.9)$$

where: A_s = spreading loss in dB

y = horizontal distance between source and receiver in m

Δh = vertical distance between rays at the receiver in m

$\Delta\theta$ = angle between rays at the source in degrees.

Figure 2.7 show the physical representation of these parameters.

The ray-trace program may also be used to calculate distances along individual paths and the time taken for a wave to propagate along this path. This means that the losses due to absorbtion, spreading and reflections may be incorporated into a ray-trace program and hence, the total loss associated with any particular ray may be calculated.

The paths most interesting to the designer of an underwater communication system are those which will travel between a particular source and receiver configuration, that is, the eigenrays of the system [8]. While there is no closed-form method to determine the eigenrays, they may be found using a ray-trace program and an iterative process. A program to compute the eigenrays using a linear approximation iteration has been written and a complete listing and flowchart appears in Appendix C. This program also computes the losses associated with each eigenray based on absorbtion, spreading and reflection

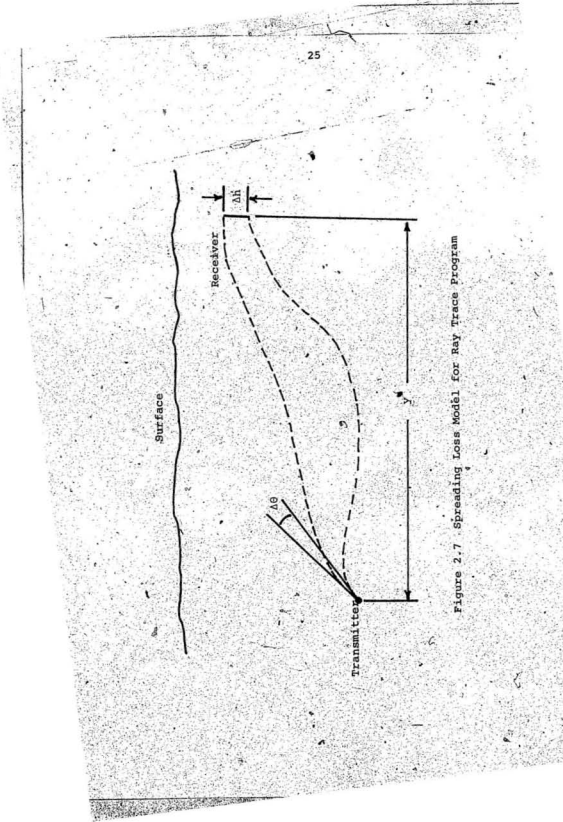


Figure 2.7 Spreading Loss Model for Ray Trace Program

losses. The output of the program is a plot of signal strength versus the travel times for each of the eigenrays, that is, the eigenray response for that particular configuration. The eigenray response for a particular ocean depth, velocity profile and source/receiver configuration is plotted in Figure 2.8. The basic ray-trace program has been used to give the visual representation of the eigenrays for this configuration which is plotted in Figure 2.9.

The eigenray program gives the designer an indication of how severe the multipath problem will be for a particular ocean configuration and also the time spread, associated with the multipath effect. This program, therefore, is a very useful tool in the design of a system which must overcome the effects of multipath.

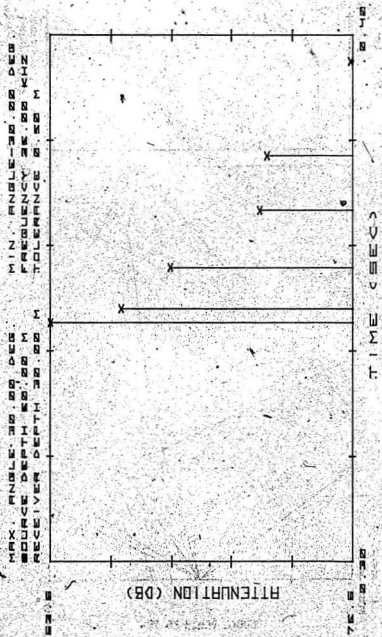


Figure 2.8 Typical Eigenray Response Program Plot

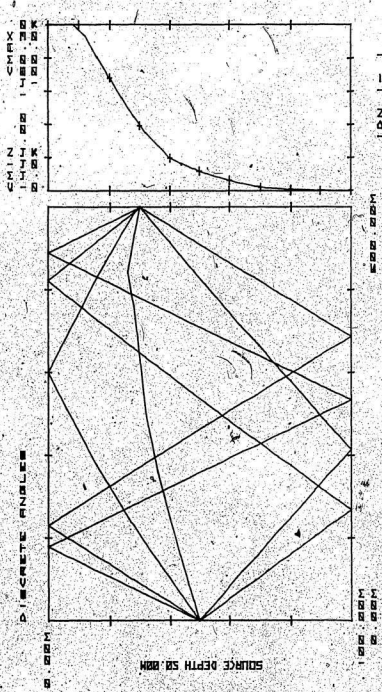


Figure 2.9 Eigenrays of Fig. 2.8 using Ray-Trace
Program

CHAPTER III

METHODS USED TO SUPPRESS MULTIPATH

3.1. Introduction

While the effect of multipath is a great hinderance to the development of a reliable underwater acoustic communication system, several systems described in the literature have been tested with varying degrees of success.[2],[3],[19],[21],[24],[31],[32],[33]. These systems have relied on one or more of four different techniques used to reduce the effects of multipath on transmission. These techniques, which will be described in turn, include transducer directivity, burst mode communication, frequency-hopping and a swept-carrier concept.

3.2 Transducer Directivity

Transducer directivity is perhaps the most obvious method of reducing the multipath effects. Since each of the eigenrays have different trajectory angles at the transmitter, a narrow beamwidth transducer could be used to allow propagation along only one path between the transmitter and receiver. This effect is shown in Figures 3.1a and 3.1b which compare the eigenray responses for a 60° beamwidth and a 10° beamwidth transmitter respectively in the same ocean configuration. As the figures show, only one path reaches the receiver for the 10° beamwidth transducer while the multipaths for the 60° beam-width transducer are quite prominent.

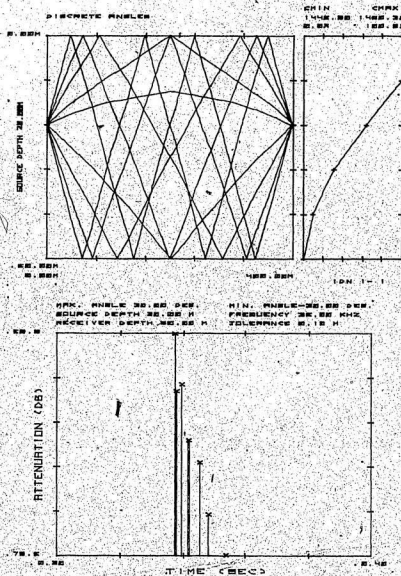


Figure 3.1a Eigenray Response for 60°
Beamwidth Transducer

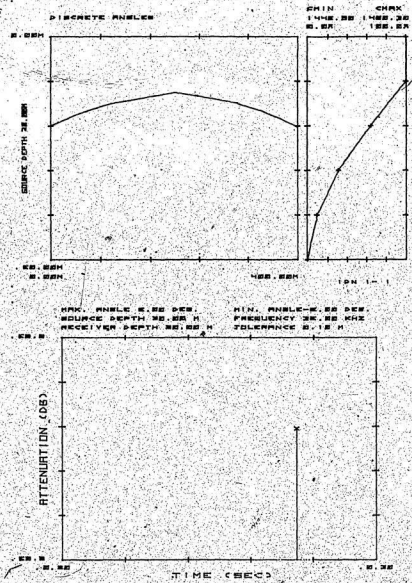


Figure 3.1b Eigenray Response for 10° Beamwidth
 * Transducer

While this method certainly has the ability to suppress multipath for horizontal transmission, it has two main problems. In the case of vertical transmission, where the receiver is directly above the transmitter or vice versa, the multipath rays all originate at the same angle and arise from reflections at the surface and bottom. This type of system must rely only on the boundary reflection losses to suppress the multipath. Another problem this technique has is transmitter/receiver alignment, particularly in a situation where the transducers are not fixed or the velocity profile changes. In these situations, a narrow beam transmitter cannot be used due to the difficulty of maintaining the receiver within the beam path.

3.3. Burst Mode Communication

The effect of multipath may be reduced by using a burst mode, whereby a message is transmitted in sections on a pulsed carrier. The key to the multipath suppression is that the carrier pulses are spaced sufficiently in time that the multipath from one pulse has died out before the next pulse is received. The pulses must also be short enough that the entire pulse is received before a multipath reaches the receiver. This type of transmission is illustrated in Figure 3.2. This is essentially the technique which is used in a sonar system. The sonar signal consists of a series of high frequency pulses, the reflections of which die out between each pulse. While this technique is effective in the suppression of multipath, it is inefficient in its

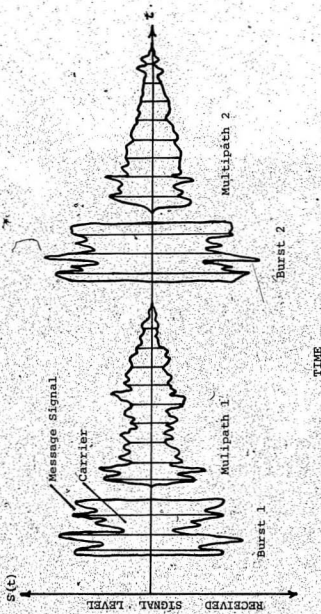


Figure 3.2 Burst Mode Communication Method

use of time, and is also a difficult technique to implement for analog messages since the transmission is not continuous. The time-efficiency depends on the geometry of the ocean but can be quite low if the multipath lasts for a long time.

3.4 Frequency - Hopping

The frequency-hopping technique may best be understood as an extension of the burst mode technique in that the message is transmitted on a pulsed carrier. Instead of just waiting for the multipath to die, however, the message is continued, but at a different carrier pulse frequency. The carrier pulse continually hops to different frequencies until the multipath from the first pulse dies out and then the sequence of frequencies is repeated as illustrated in Figure 3.3. This technique uses time efficiently, however, implementation of such a system may require quite complex circuitry. Morgera [21], for example describes a system which uses twenty different carrier frequencies and hence also requires a bank of twenty filters and a phase reference for each frequency which must be synchronized on initial contact. This technique is well suited to digital transmission, since the message data can be stopped during each hop. Analog transmission would be difficult, however, due to the interruption during each hop.

3.5 Swept-Carrier Communication

The swept-carrier concept may be considered to be an extension of the frequency-hopping technique. Instead of making

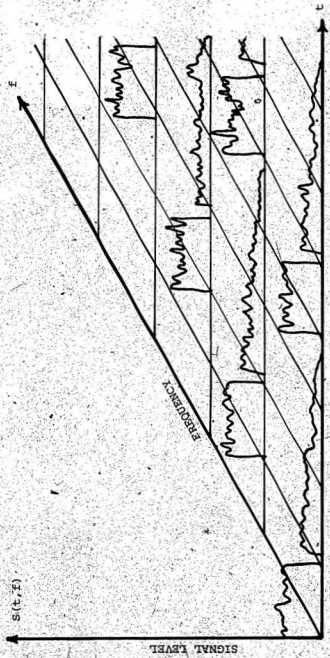


Figure 3.3 Frequency-Hopping Communication Method

many discrete jumps between carrier frequencies, however, the carrier frequency is constantly shifting as depicted in Figure 3.4. This technique has been described by Zielinski and Barbour [32], [33] and Barbour [3] and preliminary tests indicate its effectiveness in suppressing multipath. This transmission scheme creates a bandpass channel with reduced multipath noise which can be used for both analog and digital transmission. The receiver complexity inherent to a frequency-hopping technique can be reduced to a proper tracking filter. This method relies on the availability of broadband acoustic transducers for a large sweeping range. Recent work in the area of flexensional transducers may better fill this requirement for broadband transducers [18].

The tracking filter receiver may also be designed to account for some variables in the configuration such as Doppler shift due to moving transducers or varying distance between transducers.

This thesis is directed toward the development of the swept-carrier technique with particular emphasis on digital data transmission although analog voice transmission has also been considered.

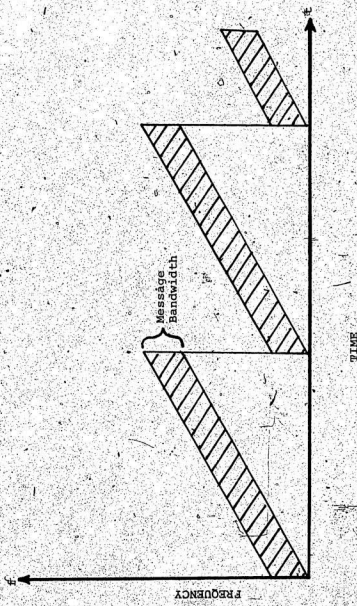


Figure 3.4 Swept Carrier Modulation Technique

CHAPTER IV

DEVELOPMENT OF A SWEEP-CARRIER SYSTEM

4.1. Design Considerations

A swept carrier communication system is designed specifically to combat the multipath effects. Each system, therefore, must be individually matched to the expected multipath conditions of the ocean model. For design purposes, the response of the ocean to an impulse will be considered to consist of a separate pulse due to the direct path, followed by a spread pulse due to the multipaths. Figure 4.1 illustrates this model and shows the parameters which describe it. These parameters include: t_0 , the arrival time of the direct path; t_1 , the arrival time of the first multipath; t_m , the total impulse response decay time. These parameters may be found using the eigenray response program if the velocity profile, ocean depth and range, relative transducer position and beamwidth are known. If the system is to be designed for use with moving transducers, then the system must be designed for the worst situation. This occurs when the time between the direct path and the multipath is short and the multipath duration is long.

4.1.1. Choice of Sweeping Waveform

Barbour [3] has considered the concept of a swept-carrier system using a carrier which is swept in a

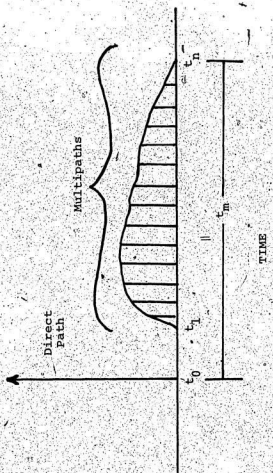


Figure 4.1 Impulse Response Model of the Ocean Channel due to Multipath

sinusoidal fashion and is tracked using a phase-lock loop. This type of sweep places the multipath carrier sweep at a certain phase separation from the direct carrier sweep and hence multipath suppression can be obtained using a tracking filter. During each cycle of the carrier sweep, however, the direct path bandwidth and the multipath bandwidth will overlap twice as shown in Figure 4.2. The time during which the bandwidths overlap depends on the phase lag and on the signal bandwidth. Barbour has shown that the optimum phase lag is 180° . If there are several multipaths, however, it is likely that there will be multipath interference at non-optimum phase lags. Barbour indicates in his conclusions that the type of sweep waveform needs more consideration.

Instead of a sinusoidal sweep, the author has considered a ramp waveform as shown in Figure 4.3. This type of sweep is more difficult to track, due to the discontinuity at the end of each period, but should give better multipath suppression. The cross-hatched areas of Figures 4.2 and 4.3 are the times during which there will be multipath interference. Clearly, this time is much less for the ramp waveform since bandwidth overlap occurs only during the quick hops at the end of each sweep. The multipath suppression for a ramp sweep would therefore be greater.

For a ramp type of sweep, the equation governing the ramp slope depends on the signal bandwidth and the time

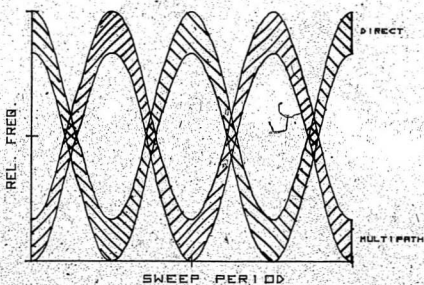


Figure 4.2 Multipath Interference of a
Swept-Carrier with Sinusoidal Sweep

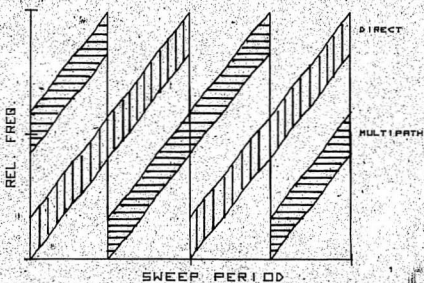


Figure 4.3 Multipath Interference of a Swept-Carrier with Ramp Sweep

separation between the direct and the multipath. Since the bandwidth of the multipath must be separate from the direct path, the minimum ramp slope is found by the equation:

$$k = \frac{B_s}{t_1 - t_0} \quad (4.1)$$

where: k = carrier sweep rate in Hz/s

B_s = signal bandwidth in Hz

t_1 = arrival time of the first multipath in s.

t_2 = arrival time of the direct path in s.

Since the multipath at any frequency must decay before the carrier can return to that frequency the minimum ramp period is equal to the total impulse response decay time t_m . The required sweep range is found simply as:

$$s_c = kt_m \quad (4.2)$$

where: s_c = carrier sweep range in Hz

k = carrier sweep rate in Hz/s

t_m = total impulse response decay time in s.

4.1.2. Carrier Frequency Selection

Having determined the required carrier sweep range, the designer must decide the position in the frequency band this range is to occupy. This decision depends on the

message bandwidth, the range of the communication system, the ambient noise and the transducers used. It may not be possible to satisfy all of the restrictions these considerations impose for all communication channels. Consequently, the designer may be forced to sacrifice message bandwidth or to allow a certain amount of multipath interference in the system.

The carrier frequency and bandwidth are related rather loosely and Carlson [5] suggests that as a rough rule of thumb:

$$0.01 < \frac{B_s}{f_c} < 0.1 \quad (4.3)$$

where: B_s = signal bandwidth in Hz

f_c = carrier frequency in Hz

This equation immediately imposes an upper and lower limit on the choice of carrier frequency. Carlson notes, however, that larger bandwidths are possible, but with reduced quality.

There is another upper limit on the carrier frequency which is imposed by the range over which the system is to operate. Since attenuation increases continuously with both range and frequency (Eqn. 2.3.), large distances restrict the designer to a low range of frequencies unless sufficient transmitter power can be obtained.

Since the main objective of a communication

system is to maximize the signal to noise ratio, the frequency spectrum of the ambient noise also plays a role in determining the carrier frequency. Figure 2.2. showed that the ambient noise is not constant over the frequency band, rather, the figure indicates a band of reduced noise in the 10kHz to 100kHz decade. The actual frequency range with maximum signal to noise level, of course, also depends on the range of the communication channel due to the frequency dependent absorption coefficient. For short distances a high range of frequencies will give the maximum signal to noise band while a long distance will require a lower range of frequencies.

Riter [23] developed an equation which gives an approximation of the optimum frequency. This equation is obtained by differentiating the sonar equation, neglecting the frequency-dependence of any unknowns. The equation Riter obtained is:

$$f_{\text{opt}} = 3.6 \times 10^5 d^{-1/2} \quad (4.4)$$

where: f_{opt} = optimum frequency in kHz
 d = range in m

The results of this equation are plotted in Figure 4.4. Riter notes that for longer ranges, slightly higher frequencies than indicated should be chosen for increased bandwidth and to eliminate low-frequency biological and man-made noises which were omitted in the equation. The optimum range for a swept-carrier system will likely fall around this optimum

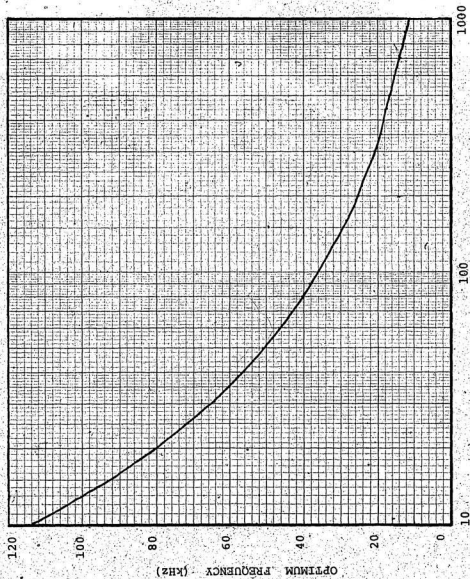


Figure 4.4 Plot of Optimum Carrier Frequency Versus Range [23]

frequency.

There is another restriction on the selection of the carrier frequency band which is imposed by the transducers. A swept-carrier system is inherently a broadband system, however, underwater acoustic transducers are resonant-type devices and are normally narrowband. Broadband transducers are generally obtained by a proper damping which in turn reduces the electro-acoustic conversion efficiency thereby increasing the required power input. By using a high carrier frequency band, however, the required damping is reduced since the resonant frequency to bandwidth ratio, that is, the Q-factor, can be increased. The need for low frequency broadband transducers with good efficiency has been recognized and research is now being directed in that area [18].

4.1.3. Ambient Noise Considerations

The main quality assessment of a communication link is in the signal-to-noise ratio. Since the ambient noise level at the receiver is fixed, the signal-to-noise ratio is governed by the source level, the attenuation and the multipath.

The required signal to noise ratio for analog signals in a particular application may be evaluated qualitatively by a comparison with conventional systems. Table 4.1. from Carlson [5] gives the signal-to-noise ratios of some conventional systems.

TABLE 4.1

Transmission Requirements for Selected Analog Signals

Signal Type	Signal-to-noise ratio, dB
barely intelligible voice	5-10
telephone quality voice	25-35
AM broadcast quality audio	40-50
high fidelity audio	55-65

House et.al. [10] developed a Modified Rhyme Test to determine the intelligibility of voice in a communication system. They reported that with a signal-to-noise ratio of 4dB, listeners made 95% correct responses.

The required signal-to-noise level for a digital system may be evaluated quantitatively by considering the allowable probability of error. Figure 4.5 from Carlson [5] shows the expected probability of error for amplitude-shift-keying and frequency-shift-keying versus the system parameter. The system parameter is related to the signal-to-noise ratio, the bandwidth and the data rate by the equation:

$$P = \frac{SNR * B}{x} \quad (4.5)$$

where: P = system parameter

SNR = signal-to-noise power ratio

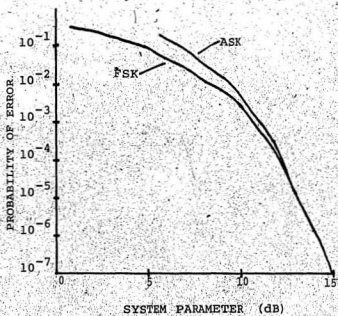


Figure 4.5 Expected Probability of Error
versus System Parameter for
ASK and FSK [5]

B = message bandwidth in Hz

r = data rate in the bit/sec

This expression is valid for an ideal receiver and represents the upper bound for the error probability of actual systems.

Once the required signal-to-noise ratio has been established, the required source level is found using the equation:

$$P_t = \text{SNR} + N + A \quad (4.6)$$

where: P_t = transmitter pressure level
in dB re 1 μ Pa at 1 m.

SNR = signal-to-noise ratio in dB

N = in-band, in-beam noise at the
receiver in dB re 1 μ Pa

A = signal attenuation from transmitter
to receiver in dB

4.1.4. Multipath Noise Considerations

Equation 4.6 only considers ambient noise in the signal-to-noise ratio. Multipath effects have not been considered since they should be removed by the swept-carrier technique. It should also be noted that the input pressure level does not affect the signal-to-multipath noise ratio since both the signal and the multipath are proportional to the input pressure. The maximum signal-to-noise ratio for an underwater system therefore is equal to the ratio of the direct path intensity to the multipath intensity. Since the multipath intensity may be comparable to the direct path intensity, the multipath effects on

the communication system may be severe. By eliminating the multipath, however, substantial improvements may be made.

The available models for multipath prediction reported in the literature [8], [15] do not provide the system designer with a simple criteria to evaluate the multipath condition, such as, the signal to multipath ratio. There is a need for a multipath model which will predict the system performance if some of the multipath components are eliminated by a suitable modulation scheme. To fill this need, the following model has been developed.

Consider the situation illustrated in Figure 4.6. A signal is transmitted from the ocean floor at depth "z" to a receiver at the surface separated from the transmitter by horizontal distance "y". The transmitted signal reaches the receiver via a direct path and also an infinite number of paths which arise from surface and bottom reflections. Associated with the reflections are the surface loss L_s and the bottom loss L_B . Assuming omnidirectional transducers, OdB source level, spherical spreading and absorbtion coefficient α , the intensity of the direct path is:

$$P_D = -[20 \log (\sqrt{y^2 + z^2}) + \alpha(\sqrt{y^2 + z^2})] \quad (4.7)$$

where: P_D = direct path intensity in dB re 1uPa

y = horizontal distance from transmitter
to receiver in m.

z = ocean depth in m.

α = absorbtion coefficient in dB/m

The intensity of any of the other paths may be found by the equation :

$$P_n = -[20 \log \{\sqrt{[(2n+1)z]^2 + y^2} l + \alpha\sqrt{[(2n+1)z]^2 + y^2} l + n(L_s + L_B)\}] \quad (4.8)$$

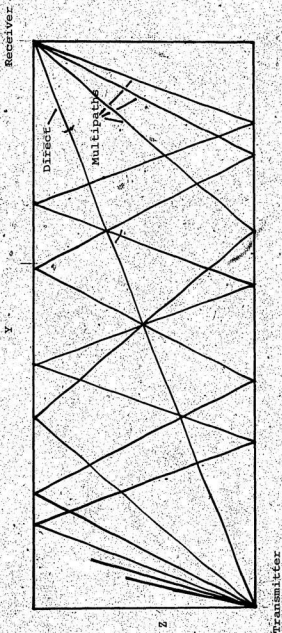


Figure 4.6 Multipaths in an Ocean of Constant Velocity.

where: P_n = intensity of the n^{th} multipath in
dB re 1μPa

n = number of surface reflections

L_s = surface reflection loss in dB

L_B = bottom reflection loss in dB

The total multipath intensity is found by assuming that the multipaths are uncorrelated, in which case their intensities add. This assumption is justified since each of the paths will be transmitting information which has been sent at different times.

The total multipath intensity is:

$$P_m = 10 \log \sum_{n=1}^m 10^{P_n/10} \quad (4.9)$$

where: P_m = total multipath intensity in dB re 1μPa

The direct to multipath intensity ratio is then:

$$\text{DMR} = P_D - P_m \quad (4.10)$$

where: DMR = direct to multipath intensity ratio
in dB

The improvement achieved by eliminating the first m multipaths assuming negligible ambient noise can be found by recalculating P_m without the contributed intensity of the first m multipaths. The improvement is found to be:

$$I = 10 \log \left[\frac{\sum_{n=1}^m 10^{P_n/10}}{\sum_{n=1}^{m-1} 10^{P_n/10} + \sum_{n=m+1}^m 10^{P_n/10}} \right] \quad (4.11)$$

where: $I = \text{improvement achieved by eliminating } m \text{ multipaths in dB}$
 $m = \text{number of multipaths eliminated}$

Equation 4.9 has been programmed on the HP9825 calculator and the output is plotted in Figures 4.7, a,b,c,d,e,f,g,h for various values of ocean depth, multipath suppression and bottom + surface reflection loss. These figures show that the improvement is greatest for vertical propagation and decreases asymptotically as the horizontal distance increases. The improvement is seen to be greater with high frequencies and high reflections losses. The improvement also increases as more multipaths are suppressed.

When the horizontal distance "y" becomes very large with respect to the depth "z", the travel distance for each path approaches "y". In this case, an interesting limit on the improvement may be found since "z" is negligible in each of the multipath intensity, P_n , calculations:

$$\lim_{y/z \rightarrow \infty} I = 10 \log \left[\frac{\sum_{n=1}^m 10^{-(20 \log(y) + ay + n(L_s + L_B))/10}}{\sum_{n=1}^m 10^{-(20 \log(y) + ay + n(L_s + L_B))/10}} \right]$$

$$= \frac{\sum_{n=1}^m 10^{-(20 \log(y) + ay + n(L_s + L_B))/10}}{\sum_{n=1}^m 10^{-(20 \log(y) + ay + n(L_s + L_B))/10}}$$

(4.12)

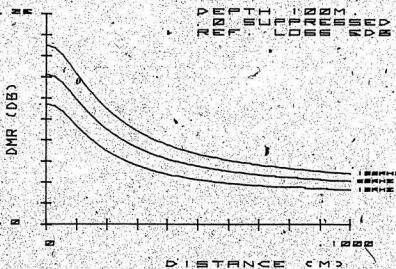


Figure 4.7a Plot of Direct to Multipath ratio versus Distance for Transmission to the Surface from a Depth of 100m.

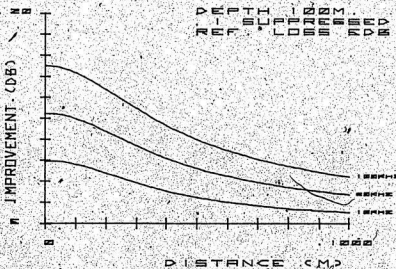


Figure 4.7b Plot of Improvement in DMR over Figure 4.7a Obtained by Suppressing the First Multipath

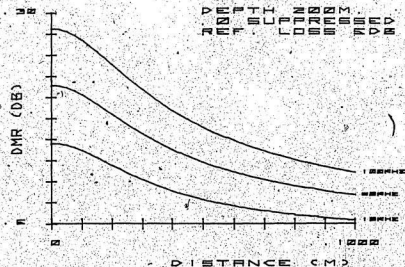


Figure 4.7c Plot of Direct to Multipath ratio
versus Distance for Transmission
to the surface from a Dept. of 200m

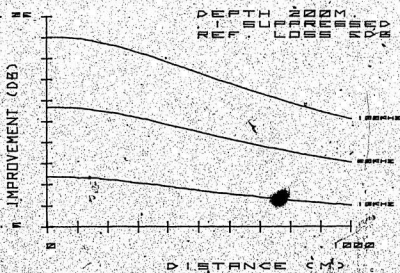


Figure 4.7d Plot of Improvement in DMR over
Figure 4.7c Obtained by Suppressing
the first Multipath

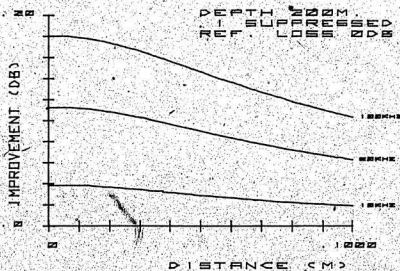


Figure 4.7e Plot of Improvement of DMR
Versus Distance with 0dB Reflection Loss

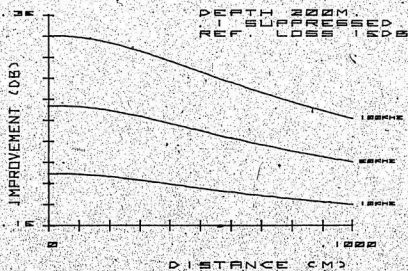


Figure 4.7f Plot of Improvement of DMR
Versus Distance with 15 dB Reflection Loss

Taking out the common factor: $20 \log y + a y$, the equation reduces to:

$$\lim_{y/z \rightarrow \infty} I = \log \left\{ \frac{\sum_{n=1}^{\infty} 10^{-n}(L_s + L_B)}{\sum_{n=1}^{\infty} 10^{-n}(L_s + L_B) - \frac{m}{L} \sum_{n=1}^{\infty} 10^{-n}(L_s + L_B)} \right\} \quad (4.13)$$

Now $\sum_{n=1}^{\infty} 10^{-n}(L_s + L_B)$ is a convergent series.

with final value $\frac{1}{10^{(L_s + L_B)} - 1}$ for all $(L_s + L_B) > 0$.

therefore:

$$\begin{aligned} \lim_{y/z \rightarrow \infty} I &= \log \left\{ \frac{\frac{1}{10^{(L_s + L_B)} - 1}}{\frac{1}{10^{(L_s + L_B)} - 1} - \frac{m}{L} \sum_{n=1}^{\infty} 10^{-n}(L_s + L_B)} \right\} \\ &= -\log [1 - (10^{(L_s + L_B)} - 1) \cdot \sum_{n=1}^{\infty} 10^{-n}(L_s + L_B)] \\ &= -\log [1 - \sum_{n=1}^{\infty} 10^{(1-n)(L_s + L_B)} + \sum_{n=1}^{\infty} 10^{-n}(L_s + L_B)] \\ &= -\log [1 - \sum_{n=0}^{m-1} 10^{-n}(L_s + L_B) + \sum_{n=1}^m 10^{-n}(L_s + L_B)] \\ &= -\log [1 - 10^{-0}(L_s + L_B) + 10^{-m}(L_s + L_B)] \\ &= -\log [1 - 10^{-m}(L_s + L_B)] \\ &= m(L_s + L_B) \end{aligned} \quad (4.14)$$

The improvement, therefore asymptotically approaches a value which depends only on the reflection losses and the number of paths suppressed. This asymptotic approach to the value $m(L_s + L_B)$ is shown in Figures 4.7. The improvement in signal-to-noise ratio to be gained by multipath suppression is seen to be quite substantial.

4.1.5 Choice of Modulation Technique

The swept carrier technique will provide a bandwidth with reduced multipath interference. The designer must now decide which modulation technique will be used to shift the message to this bandwidth. An important factor in the selection of the modulation type is the availability of the carrier component. In a situation in which the transducers are not fixed, the Doppler shift will affect the expected carrier frequency of a swept-carrier system. Unless the carrier component is available to be tracked, compensation for the Doppler shift would be difficult and distortion of the message signal would result. Some of the conventional modulation techniques such as FM, PM, DSBSC and SSB do not contain the carrier component and hence are not well-suited to this task.

Two possible choices remaining are AM or SSB with a reinserted carrier. While SSB has an advantage over AM in reduced power and bandwidth requirements for the same message bandwidth, the modulator and demodulator are more complex [13], [25]. For this reason, amplitude modulation was chosen to impress the message on the swept-carrier.

4.2 Prototype Design

4.2.1 Introduction

In order to test the concept of a swept-carrier communication system, a prototype was designed and built. This system is designed to send either analog or digital messages from the ocean floor at a depth of 100m - 300m to a receiver near the surface over a range of 1000m as illustrated in Figure 4.8. The system provides a 2kHz message bandwidth in which the multipath is suppressed. This bandwidth is amplitude modulated onto a swept-carrier having a ramp function sweep. The receiver tracks the sweeping carrier and demodulates the message. Circuitry has also been implemented which will account for Doppler shift, hydrophone movement and carrier synchronization. The system is adaptable to many channel requirements since the carrier frequency, frequency range and the ramp period are adjustable.

Analog messages are generated in the transmitter by a microcassette recorder which is encased in the transmitter housing. Digital messages are generated by an 8-bit pseudo-random data word generator. The data words are controlled at both the transmitter and receiver by universal asynchronous receiver/transmitters (UART).

The transmitter consists of a hydrophone, a power amplifier board, a swept-carrier modulator, a data generator, and a microcassette player. The circuits are built on

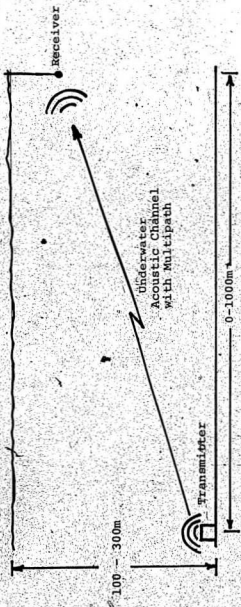


Figure 4.8 Ocean Configuration for Prototype System

4" x 4" circuit boards which are powered by two 12 volt rechargeable batteries, all of which is enclosed in a stainless steel housing. Figure 4.9. shows the transmitter without the stainless steel housing.

The receiver consists of a hydrophone, a pre-amplifier, an adjustable filter/amplifier and a demodulator. The receiver requires an outside power source of + 12v.

Both the power amplifier and the preamplifier have been designed by Ametek of California. The circuit diagrams for these amplifiers are found in Appendix D.

4.2.2. Swept-Carrier Modulator Board

The circuitry of the swept carrier modulator accepts an input signal, either analog or digital, and heterodynes the signal to a sweeping carrier frequency using amplitude modulation. This board also generates the ramp which controls the carrier frequency. Figure 4.10 shows the block diagram of the swept-carrier modulator board. The circuit diagram and tuning procedure is found in Appendix D. The ramp period, carrier frequency range, carrier frequency position, and the modulation depth are adjustable on this board.

4.2.3 Data Generator Board

The data generator board is used to provide a pseudo-random sequence of 8-bit data words for transmission as shown in the block diagram of Figure 4.11. The sequence of

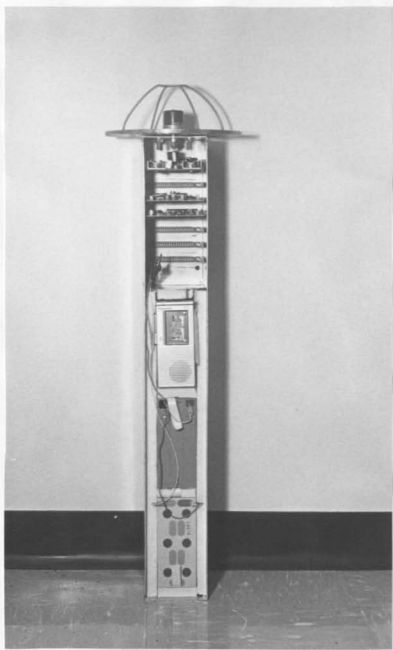


Figure 4. 9 Prototype Transmitter showing Hydrophone, Circuitry, Tape Recorder and Batteries

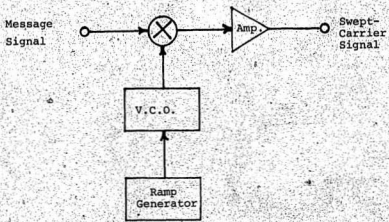


Figure 4.10 Block Diagram of Swept-Carrier Modulator Board

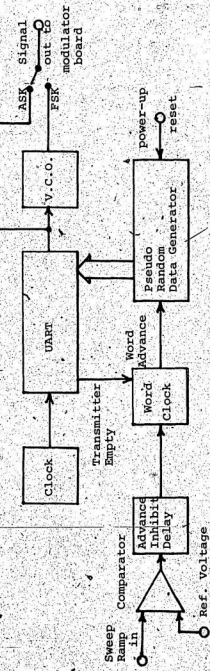


Figure 4.11 Block Diagram of Pseudo-random Data Generator Board

words is generated using Exclusive OR feedback on a clocked 7 stage shift register as shown in Fig. D.1d.. This provides 255 words in a random order. In this arrangement, if the data word was ever 11111111, the feedback circuitry would never change the word. To eliminate this problem, the shift register is reset on power-up to 00000000 and consequently the word with all 1's never occurs. The word sequence is advanced by a word clock which sets the time between words. Circuitry has also been implemented which stops the data generation during the fall time of the ramp, that is, the carrier frequency hop since the receiver is not able to demodulate the data during this time.

The 8-bit word is gated to the UART and then organized into serial format for transmission. The UART adds start and stop bits in order that the transmission can be asynchronous and also generates a parity bit for error detection. The bit rate from the UART is set by an external clock which runs at $16 \times$ the bit rate. Data to the swept-carrier modulator may be either ASK or FSK depending on the jumper position. The bit rate, time between words, time during which data is stopped to allow for the carrier frequency hop, and the reference voltage at which the data is stopped are adjustable on this board. The circuit diagram and adjustment procedure for the data generator board is found in Appendix D.

4.2.4 The Receiver

Perhaps the most critical section of the

swept-carrier system is the receiver. The receiver must accurately demodulate the message signal from a sweeping carrier. This signal may be distorted by non-linearities in the amplifiers and transducers, frequency shifted by the Doppler effect and distorted by multipath. The receiver must be able to synchronize with the sweeping carrier on initial contact and maintains synchronization through Doppler shifts and through momentary losses of signal. The receiver circuitry also includes the necessary circuitry to demodulate FSK and ASK data. A block diagram of the receiver which the author has designed to accomplish the task is illustrated in Figure 4.12. The circuit diagram and tuing procedured are included in Appendix D.

The front end of the receiver uses a Rockland 442 HiLo filter/amplifier which filters the received signal from the pre-amplifier to remove noise outside the swept-carrier range. The automatic gain control then assures the input maintains a constant signal level for the rest of the receiver. The signal level of an underwater communication system can vary quite substantially as a hydrophone moves through the standing waves caused by the multipath. In addition to this effect, however, the automatic gain control of a swept-carrier system must account for the frequency dependent signal absorption and the transducers transmitting and receiving frequency responses. The automatic gain control must quickly respond to the fluctuating signal level to maintain a constant input level for the demodulator. The AGC used in this design features a fast attack with a slow decay time constant of 200ms with a 40 dB

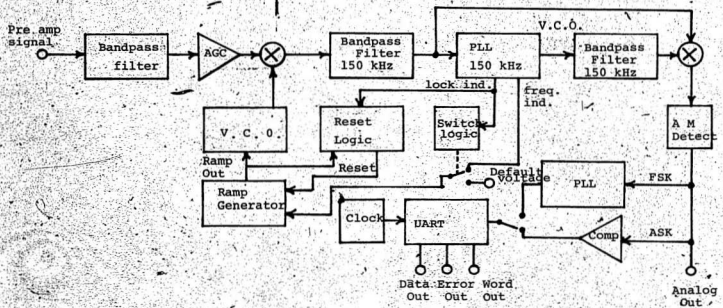


Figure 4. 12 Block Diagram of Receiver

range extending to 50kHz. The decay time constant had to be increased to 2s for the ASK signal, however, to account for the word separation time. While it may be desirable that the AGC act quickly, it should be realized that on AGC is a multiplier and as such is amplitude modulating the signal. This leads to a frequency smear of the signal and consequently introduces distortion which places a lower limit on the response time of the automatic gain control.

In order to track the carrier, it is necessary that the sweeping carrier be heterodyned to a constant intermediate frequency. This is accomplished by multiplying by a local oscillator which sweeps at the same rate and over the same range as the swept carrier. The frequency of the local oscillator is given by the equation:

$$f_{LO}(t) = f_{IF} + f_C(t) \quad (4.15)$$

where: $f_{LO}(t)$ = instantaneous local oscillator frequency, in Hz

f_{IF} = intermediate frequency in Hz

$f_C(t)$ = instantaneous carrier frequency in Hz

There is a restriction placed on the choice of f_{IF} which arises from the facts that the multiplier is not perfect and there are distortions of the received signal due to nonlinearities in the amplifiers and transducers. This restriction was discovered when interfering frequencies were found at the multiplier output. A real multiplier suffers from feedthrough and may be modelled as shown in Figure 4.13. As a result of this

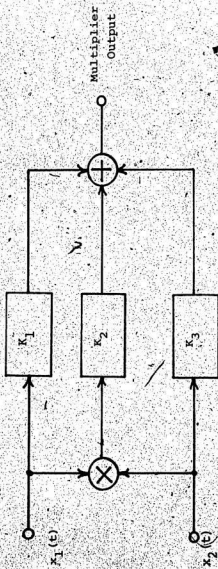


Figure 4.13 Block Diagram of Real Multiplier

imperfection, extraneous frequency components appear at the output. When one of the inputs contains a harmonic, as will the swept carrier, additional frequencies are created. The frequencies resulting from a sweeping carrier $f_C(t)$ with a second harmonic, being multiplied by a local oscillator $f_{LO}(t)$ are catalogued in Table 4.2 and the separation from the required f_{IF} is calculated using Eqn. 4.15.

TABLE 4.2

Catalogue of Multiplier Output Frequencies and their Separation from the Intermediate Frequency

<u>Multiplier Output Frequencies</u>	<u>Separation from f_{IF}</u>
$f_C(t)$	$f_{IF} - f_C(t)$
$2f_C(t)$	$f_{IF} - 2f_C(t)$
$f_{LO}(t)$	$f_C(t)$
$f_{LO}(t) - f_C(t)$ (desired)	0
$f_{LO}(t) + f_C(t)$	$2f_C(t)$
$f_{LO}(t) - 2f_C(t)$	$f_C(t)$
$f_{LO}(t) + 2f_C(t)$	$3f_C(t)$

From the table it can be seen that the overall maximum obtainable separation is equal to $f_C(t)$, the lowest carrier frequency. This separation may be less, however,

depending on the choice of f_{IF} . The feedthrough of the carrier second harmonic, second in the table, when multiplied by the local oscillator may produce an interfering frequency near the intermediate frequency. In order to maintain the maximum separation, f_{IF} must be chosen such that:

$$f_{IF} \geq 2f_H + f_L \quad (4.16)$$

where: f_H = highest carrier frequency in Hz

f_L = lowest carrier frequency in Hz

The intermediate frequency for this receiver has been chosen at 150kHz which should be adequate for a wide range of carrier frequencies.

The intermediate frequency is maintained using a phase lock loop which adjusts the sweep rate of the ramp controlling the local oscillator. If the signal is lost momentarily, and consequently the phase lock loop loses lock, the ramp rate control is switched to a default voltage which maintains the ramp rate at the expected value. Control is again returned to the phase lock loop when it regains lock.

Since the receiver does not have any a priori indication of the carrier frequency at any time, circuitry must be incorporated which will allow the local oscillator to synchronize with the sweeping carrier. This is accomplished by maintaining f_{LO} at $f_L + f_{IF}$ until the intermediate frequency phase lock loop indicates that lock has been established. This indicates that the sweeping carrier is at its lowest frequency and the local oscillator is freed to follow it.

Should the IF phase lock loop lose lock momentarily, the default voltage will maintain the sweep of the local oscillator at the expected rate. If, however, the lock is lost for a substantial period of time, say in the order of one sweep, a slight variation in the sweep rate of the transmitter and receiver could put the local oscillator out of sync with the carrier when the signal is again restored. Logic to cover this possibility has been implemented. As shown in Figure 4.14, if the receiver loses lock during the stop portion of the sweep range, the local oscillator will be set to wait for the lowest carrier frequency again. When lock is restored at this frequency, the local oscillator is again freed to follow the carrier.

Using the phase lock loop to track the intermediate frequency has an advantage in that the voltage controlled oscillator output can be used for synchronous AM demodulation of the intermediate frequency. The output of the demodulator is then filtered by a lowpass filter and the message is recovered. The main suppression of the multipath is achieved by this lowpass filter since the multipath is not within the signal bandwidth surrounding the intermediate frequency. By suppressing the multipath at this point, rather than at a higher frequency stage, a sharper cut off can be achieved for the same Q factor on the filter.

At this stage, the analog message has been recovered. If the message is digital, a comparator for ASK or a phase lock loop for FSK provide the final input to the receiving

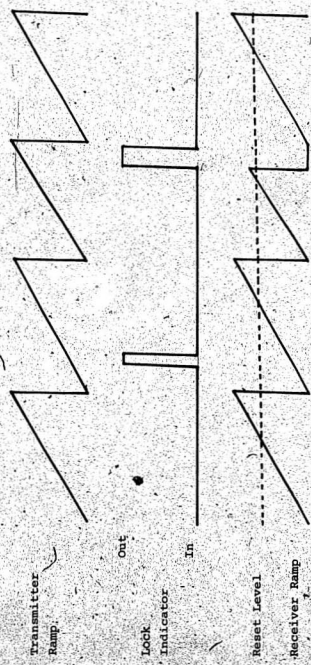


Figure 4.14 Diagram of Receiver Synchronization Logic

UART. This UART takes in the serial data word and provides a parallel output. It also checks parity and indicates parity errors. The word count output can be used to determine the probability of error for the system.

Since an even number of bit errors will not cause a parity error indication but any odd number will:

$$W = 9P_E - 72P_E^2 + 261P_E^3 - 558P_E^4 + 774P_E^5 \\ - 720P_E^6 + 450P_E^7 - 180P_E^8 + 37P_E^9 \quad (4.17)$$

where: W = percentage of words with parity errors.

P_E = actual probability of error in a bit.

For $P_E \ll 1$ the bit error probability rate is:

$$P_E = \frac{W}{9} \quad (4.18)$$

4.2.5 Transducer Selection

The transducers selected for the prototype are ITC 3147A model hemispherical transducers. Since the system is designed to transmit from the ocean floor to the surface, there is no need to use omnidirectional transducers. The transmitter need only transmit in the upward hemisphere and the receiver need only receive in the downward hemisphere. This gives the advantage of being able to attenuate the surface reflected

multipath using the transducer directivity, thereby reducing the required sweep rate by increasing the time between the direct path and the multipath (Eqn. 4.1). These transducers, when attached to the housing have a back receiving response of -16 dB relative to the forward response.

The transducers have a 10 dB operating range from 16 kHz to 46 kHz as seen in the curves of Appendix E.

While the transducers cover the required frequency range, the frequency response was found to be too "peaky" for use in a swept-carrier system. This effect was discovered during sea trials and is detailed in Section 4.3. Therefore this is not the best selection of transducers.

4.2.6 Prototype Housing

The prototype transmitter is encased in a capped stainless steel, 6" diameter schedule 42 pipe which contains the batteries, tape recorder and circuitry. The transducer is attached outside the housing. The transmitter is suspended in a tripod stand on a gimbal. This gimbal ensures that the transmitter points upward independent of the ocean floor slope. The transmitter housing and tripod are shown in Figure 4.15.

The receiver hydrophone is attached outside the receiver housing which contains the preamplifier. The receiver preamplifier housing is also constructed of a capped stainless steel schedule 42 pipe. The output signal of the preamplifier passes through a cable to the onboard receiver. Figure 4.16

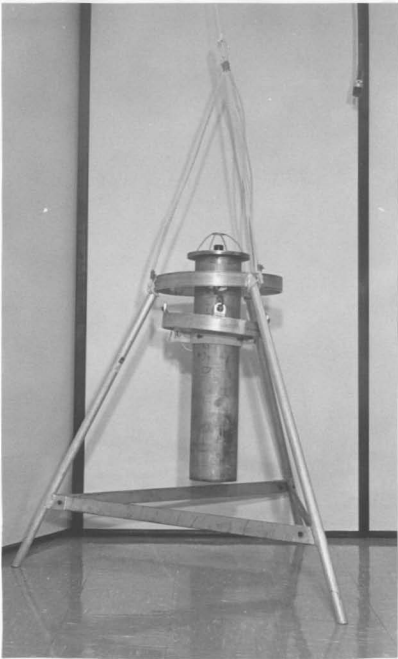


Figure 4.15 Transmitter Mounted in Tripod
on Gimbal

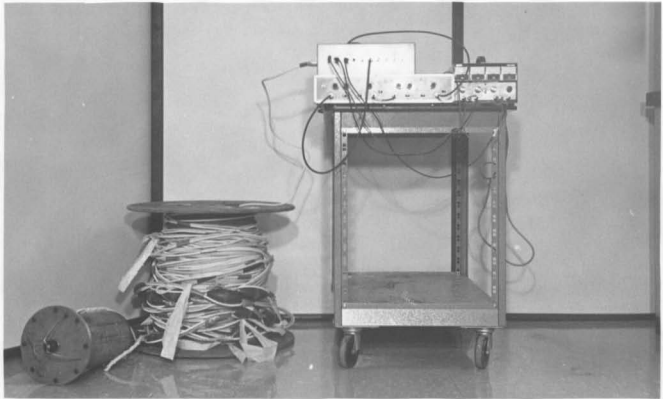


Figure 4. 16 Receiving System, Hydrophone, Cable
and Onboard Circuitry

shows the hydrophone, cable, and onboard receiver.

Both the transmitter and receiver housings are capable of sustaining the water pressure to 600 m.

Space has also been allocated in each of the housings for expansion, possibly to a two-way communication test system.

4.3 Prototype Testing

4.3.1 Laboratory Testing

The swept carrier prototype has been tested in the laboratory in the set-up depicted in Figure 4.17. The results of the frequency response test of the system are found in Figure 4.18. The high frequency cutoff at 2200 Hz is due to the lowpass output filter. The low frequency is limited to about 20 Hz due to the automatic gain control.

Without outside interference, voice transmission was found to be highly intelligible with the only fault being a "click" during each frequency hop at the end of a ramp. This "click" was similar to a scratch on a record.

Data transmission was also good having a probability of error in the order of 10^{-5} for either FSK or ASK with a 500 bps data rate.

The effectiveness of the receiver in suppressing multipath was also evaluated using a multipath simulator shown

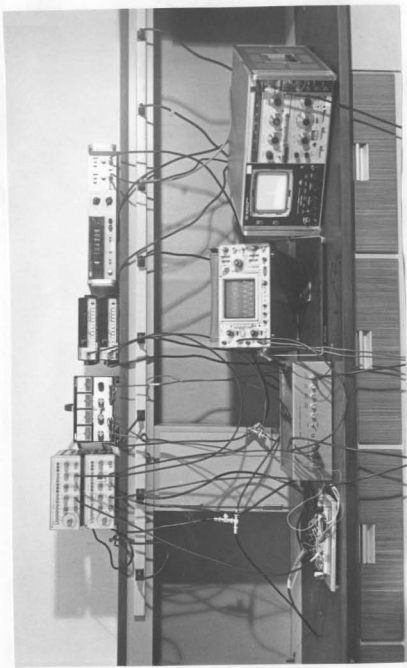
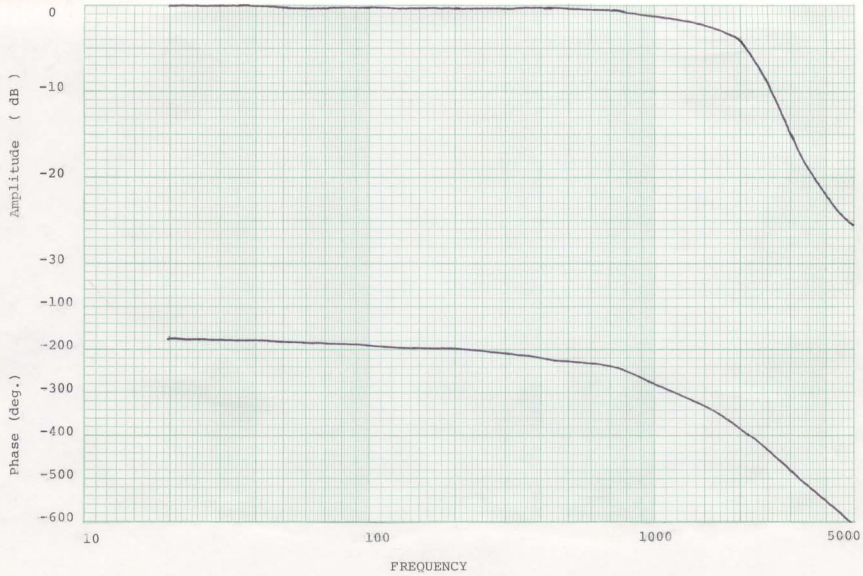


Figure 4.17 Laboratory Test Set-up



in Figure 4.19. The multipath simulator generates two ramp signals with an adjustable phase shift between them. These ramps are used to control the voltage controlled oscillators of two HP3312A function generators. The signal from each of the oscillators is a swept carrier which is capable of being amplitude modulated.

To test the multipath suppression, one of the carriers was modulated by a 1000Hz sine wave and the other was modulated by a 1400 Hz sine wave. The modulation index for each carrier was 50%. The carriers were swept over a 20 kHz to 40 kHz range on a 500 ms cycle. The carrier amplitudes were equal and the suppression was measured as the ratio of the 1400 Hz and 1000 Hz signals at the receiver output. The phase shift between the ramps was then adjusted to determine the multipath suppression obtained versus the separation between the ramp sweeps. The results of this test are tabulated in Table 4.3.

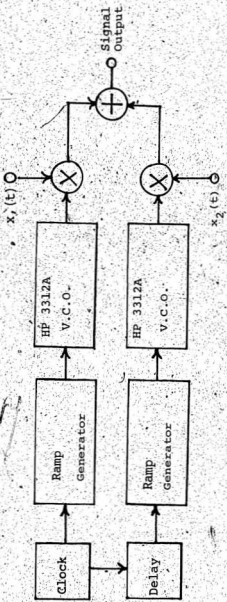


Figure 4.19 Block Diagram of Multipath Simulator

TABLE 4.3

Multipath Supression Obtained for Various Separations
between Two 500 ms Ramps

Separation (mS)	Multipath Supression (dB)
50	2
100	5
150	10
200	19
250	24
300	24
350	16
400	10
450	0

These results clearly show that the multipath suppression is greatest in the 180° phase shift region. This suppression drops as the multipath channel carrier frequency approaches that of the direct path. As the bandwidths of the direct and multipath channels begin to overlap, of course, the suppression drops to 0dB.

These tests indicate that the prototype is capable of providing a 2 kHz message bandwidth in which the multipath effects are suppressed.

4.3.2. Sea Trials

The system prototype has been tried in a series of vertical propagation tests through 100 m of water in Conception Bay. The tests were designed to compare the performance of a swept carrier system to that of a conventional amplitude modulated constant carrier. These tests involved: an evaluation of the multipath condition; a comparison of the amplitude fluctuations of a swept carrier and a constant tone; a comparison of voice transmission using a swept carrier and a constant carrier using a Modified Rhyme Test; and a comparison of data transmission capability using ASK and two tone AM (FSK on AM). The same system was used for both the swept carrier and the constant carrier since a conventional system could be tested simply by stopping the sweep function in the transmitter and receiver and tuning both to the desired frequency. The carrier frequency used in this case was 35 kHz. The modulation index used in both cases was 50%. The test scenario is depicted in Figure 4.20.

To obtain a message bandwidth of 2 kHz, the minimum carrier frequency used was 20 kHz. The maximum carrier frequency was limited by the transducer frequency response to 40 kHz. Since the surface reflected multipath was to be attenuated by the transducer directivity, the first multipath to be suppressed by the swept carrier occurs after a surface and a bottom reflection. This multipath will have travelled through a

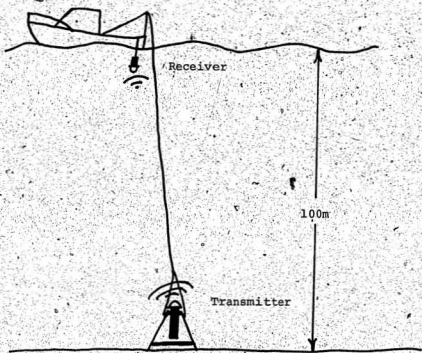


Figure 4.20 Sea Trial Test Scenario

distance which is greater than the direct path by a distance equal to twice the depth. Given a sound velocity of 1500 m/s this corresponds to a separation of 0.13 s between the direct path and the multipath. From Eqn. 4.1, the minimum sweep rate is:

$$k = \frac{4 \text{ kHz}}{.13} = 30 \text{ kHz / sec}$$

X
The actual sweep rate chosen was 40 kHz/s for a 500 ms sweep period. This rate gives a better multipath rejection as shown in Table 4.3. The second and third multipaths, that is after two and three surface and bottom reflections, should also be suppressed since they occur within 400 ms after the direct path.

The expected noise level was 48 dB relPa from the curves of Figure 2.2 using 4 kHz bandwidth. With a directivity index of 4 dB, the in-band, in-beam noise was predicted as:

$$N = 48 - 4 + 10 \log 4000 = 80 \text{ dB re } 1 \mu\text{Pa}$$

In order to ensure that interference was due to multipath, rather than to ambient noise, the signal was transmitted at sufficient level for a 40 dB signal to ambient noise ratio. This required a signal level at the receiver of 120 dB re 1 μPa . Assuming spherical spreading and an expected absorbtion coefficient of 0.008 dB/m, the transmission losses were calculated to be:

$$A = 20 \log 100 + .008 \times 100 + 41 \text{ dB}$$

Using the transducer response curves, the required voltage for the transducer was found to be:

$$V_{\text{rms}} = 10 \frac{120 + 41 - 130}{20} = 35 \text{ V}_{\text{rms}} \text{ or } 100 \text{ V}_{\text{pp}}$$

The actual signal to ambient noise ratio during the test was found to be approximately 35 dB.

The multipath was evaluated using the envelope of the 50kHz pulse from a depth sounder. Figure 4.21 shows the envelope of the received echoes. As expected, the multipath causes a series of pulses separated by 0.13 sec. In this figure, the first pulse is received directly from the depth sounder, attenuated by the back receiving response of the hydrophone. The second pulse has undergone one bottom reflection and shows some pulse elongation due to the overlapping surface reflection. The third pulse represents one surface and two bottom reflections. The sequence then repeats as a new pulse is transmitted.

The tests for data transmission capability using a conventional AM system showed that the multipath did indeed degrade the transmission severely. With a signal to ambient noise ratio of 35-dB, and a bit rate of 500 bits/sec, the error rate for ASK was found to be only 0.63 while the FSK on AM was only slightly lower at 0.61. Voice transmission using AM over the 100 m was found to be just barely intelligible. This poor quality of transmission indicates that the indeterminate nature of multipath interference severely limits the reliability of conventional

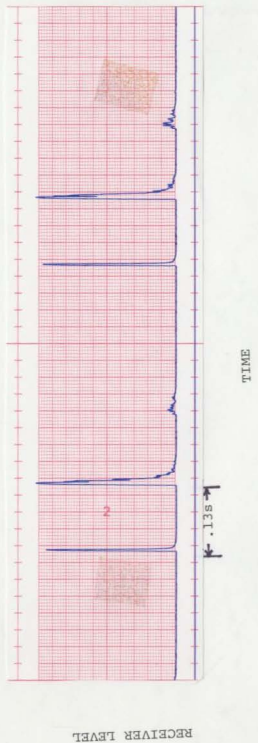


Figure 4.21 Sea Trial Multipath Condition

communication techniques in the ocean environment.

The swept carrier system did not perform as well as expected. The error rates for both ASK and FSK on AM was found to be about 0.60 and the voice intelligibility was found to be slightly worse than for the conventional AM. The reason for this poor quality transmission was determined to be due to the frequency response of the transducers.

Figure 4.22 and Figure 4.23 compare the amplitude fluctuations of a constant 35 kHz tone and the swept carrier, with a constant source voltage transmitted through 100 m of water to the surface. It is evident that the frequency response of the transducer has much more of an influence on the amplitude fluctuation than does the multipath interference.

Since the AGC must provide a constant input signal to the receiver, it is effectively multiplying by the reciprocal of the amplitude fluctuation. Spectral analysis using a Fourier analyser indicates that for the constant tone the frequency components of the reciprocal of the amplitude fluctuation are below 1Hz as shown in Figure 4.24. The spectrum of the AGC multiplier for the swept carrier, however, from Figure 4.25, has frequency components up to 10Hz with the sweep frequency of 2 Hz and harmonics being prominent. Since multiplication in the time domain represents a convolution in the frequency domain, the AGC introduces a 10Hz frequency smear into the signal, which severely distorts the signal.

This distortion due to the amplitude fluctuation of the transducer response can be eliminated by using

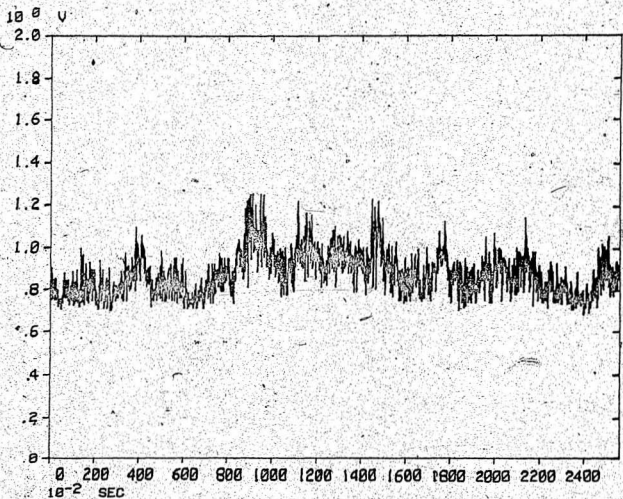


Figure 4.22 Amplitude Fluctuation of constant
35 kHz tone due to Multipath

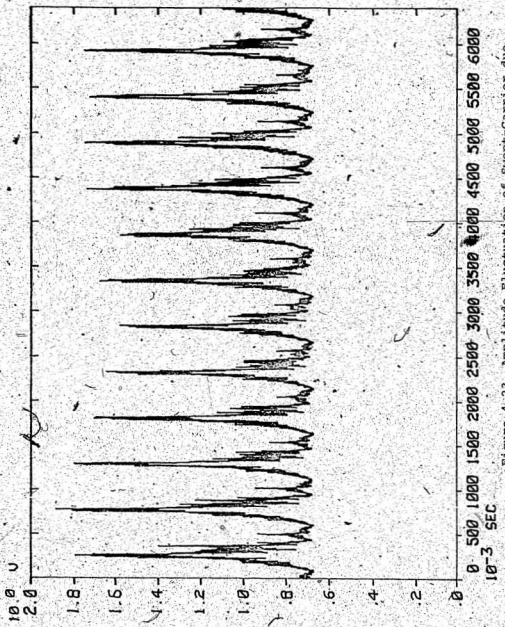


Figure 4.23 Amplitude Fluctuation of Swept-Carrier due to Multipath and Transducer Response

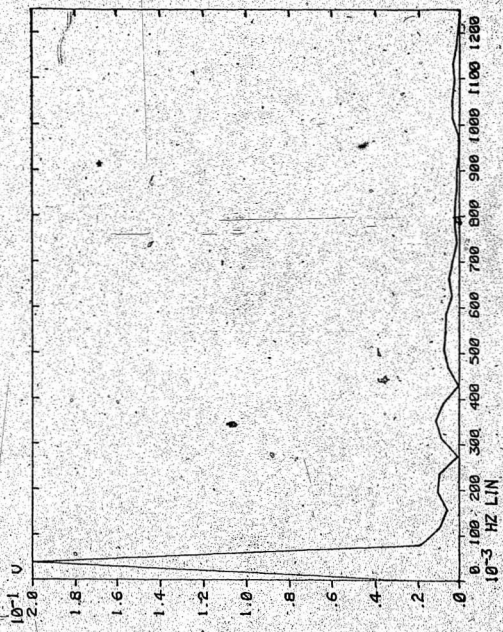


Figure 4.24 Spectral Component of AGC Effect
for Constant Carrier

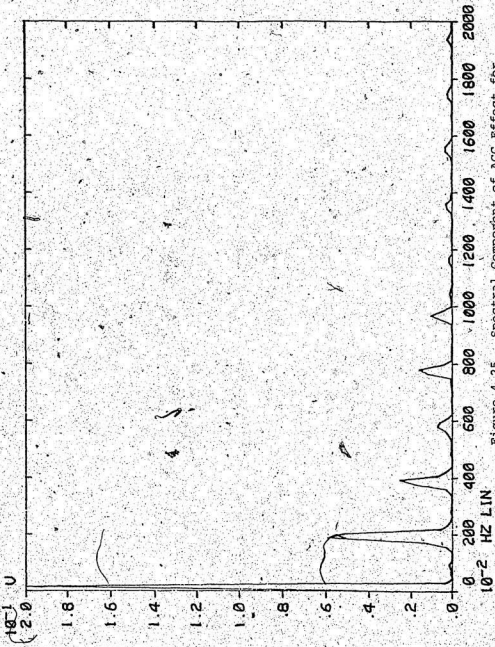


Figure 4.25 Spectral Component of AGC Effect for
Swept-Carrier

transducers which have a much flatter response. Alternatively, filters may be incorporated at the transmitter and receiver which will compensate for the frequency response of the transducers over the sweep range to give a flat acoustic frequency response. Unless the effect of the transmitter frequency response is accounted for, the swept carrier system is limited to use in situations which require slow sweep rates. In these cases, the frequency smear caused by the AGC will be small.

CHAPTER V

CONCLUSIONS

It has been shown that considerable improvement in the signal to noise ratio of an underwater communication system may be obtained through multipath suppression. As a result of this improvement, the reliability of the system is increased and higher data rates may be obtained for a given probability of error. The required multipath suppression may be realized through innovative modulation techniques, such as using a sweeping carrier.

Laboratory tests of a swept carrier prototype have indicated that such a system can effectively suppress the multipath interference inherent in an underwater acoustic channel. Sea trials, using the prototype system were not entirely successful. The prototype did not function properly due to the "peaky" nature of the transducer frequency response. Since a swept carrier system must be broadband, transducers which exhibit a flat frequency response must be used to provide an acoustic signal of constant amplitude. Alternatively, filters may be designed which will compensate the transducer response and thereby artificially produce a flat response. Unless the frequency response is flat, the system is restricted to a very slow sweep which may be compensated by an AGC with a slow response. The

multipath conditions encountered in ocean depths of 100-300 m are such that the time separation between the direct and multipath signal is small. This necessitates the high sweeping rates which can not be properly compensated for using an AGC when combined with non-uniform frequency responses of acoustic transducers.

Some further changes may be implemented in the system design to improve the performance. To increase the data rate, the pulses used for the ASK system can be shaped to raised cosine pulses which will reduce the effects of intersymbol interference at the receiver [25]. To reduce the probability of error, the UART in the receiver can be exchanged for one which samples more than once per bit. Finally, a bandpass filter should be designed and installed in the system to replace the Rockland HILO filter which is now being used as part of the receiver.

These modifications should lead to a further reduction in the system probability of error and future sea trials should indicate the effectiveness of a swept carrier system in reducing the multipath interference.

BIBLIOGRAPHY AND LIST OF REFERENCES

1. Anderson, V.C.: Acoustic communication is better than none. IEEE Spectrum. October 1970. pp 63-68
 2. Andrews, R.S. and Turner, L.F.: On the Performance of Underwater Data Transmission Systems Using Amplitude-Shift-Keying Techniques. IEEE Trans. on Sonics and Ultrasonics. Vol. SU-23, January 1976, pp. 64-71
 3. Barbour, R.L.: Underwater Acoustic Swept Carrier Communications. M. Eng. Thesis, Memorial University of Newfoundland. April 1979.
 4. Bohman, C.E. and Jackson, D.E.: Underwater Acoustic Communications. Sperry Tech. Vol. 1, 1973., pp 10-15
 5. Carlson, A.B. : Communication Systems; An Introduction to Signals and Noise in Electrical Communication. New York: McGraw Hill, 1968.
- Clay, C.S. and Medwin, H. : Acoustical Oceanography; Principles and Applications. New York, N.Y.: John Wiley & Sons, 1977.

7. Dunbar, R. and Holmes R.: Towards Tetherless Unmanned Submersibles. Underwater Systems Design. June/July 1980. pp. 11-15
8. Gerlach, A.A. : Acoustic Transfer Function of the Ocean for a Motional Source. IEEE Transactions on Acoustics, Speech, and Signal Processing, Vol. ASSP-26, No. 6, 1978. pp 493-501
9. Goddard, G.C. : An Underwater Acoustic Telemeter for use in a Multipath Channel. Ph. D. Thesis, University of Birmingham. April 1970.
10. House, A.S. et. al. : Articulation - Testing Methods: Consonantal Differentiation with a Closed Response Set. J. Acoust. Soc. Am., Vol. 37, No. 1, 1965. pp. 158-166
11. Hummels, D.R. : The Capacity of a Model for the Underwater Acoustic Channel. IEEE Trans. on Sonics and Ultrasonics, Vol. SU - 19, No. 3, 1972. pp. 350-353
12. Knudsen, V.O. et. al. : Underwater Ambient Noise. J. Marine Research, Vol. 7, No. 3, 1949. pp 410-429

13. Kurth, C.F. : Generation of Single-Sidelobed Signals in Multiplex Communication Systems. IEEE Trans. on Circuits and Systems, Vol. CAS-23, No. 1, 1976. pp 1-17
14. Leroy, C.C. : Development of Simple Equations for Accurate and More Realistic Calculation of the Speed of Sound in Seawater. J. Acoust. Soc. Am., Vol. 46, No. 1 (Part 2) 1969. pp 216-226
15. Lord, G.E. and Plemos T.D. : Characterization and Simulation of Underwater Acoustic Signals Reflected from the Sea Surface. J. Acoust. Soc. Am., Vol. 63, No. 2, 1978. pp 378-385
16. Lytle, D.W. : Characteristic Problems of Underwater Communications. IEEE Int. Conf. on Communications, Vol. 2, Seattle Wash. 1973. pp 38/1-3
17. Marsh, D.E. and Rowlands R.O. : Upper Bounds on the Information Rate for Underwater Acoustic Communication. IEEE National Telemetering Conf. Record., New York, 1968. pp 308-313

18. Marshall, W.J. et. al. : Advances in Flexensional Transducer Design. Proc. of Oceans '79 Int. Conf., San Diego, 1979. pp 124-129
19. Miller, C.S. and Bohman C.E. : An Experiment in High Rate Underwater Telemetry. IEEE Int. Conf. on Engr. in the Ocean Environment, Newport 1972. pp 34-38
20. Morgera, S.D. : Small Submersible Acoustic Communications System Design. Proc. of Oceans '78 Int. Conf., Wash. C.D., Sept. 1978. pp 66-71
21. Morgera, S.D. : High Data Rate Acoustic Telemetry. Proc. of Oceans '79 Int. Conf., San Diego, 1979. pp 130-136
22. Riter, S. : Pulse Position Modulation Communications Via the Underwater Acoustic Communication Channel. SWIEECO Record of Technical Papers of the 22 Southwestern IEEE Conference and Exhibition Dallas, Texas, 1970. pp 453-457
23. Riter, S. : Underwater Acoustic Telemetry. Offshore Technology Conf., Houston, Texas 1970. pp 465-474

24. Ryerson, D.E. : A High Data Rate Underwater Acoustic Telemetry System. Proc. of Oceans '80 Int. Conf., Seattle, Washington, 1980. pp 259-262
25. Schwartz, M. : Information Transmission, Modulation and Noise. New York, N.Y. : McGraw-Hill 1970.
26. Tucker, D.G. and Gazey, B.K. : Applied Underwater Acoustics. London, U.K. : Pergamon Press, 1966.
27. Urick, R.J. : Principles of Underwater Sound. New York, N.Y. : McGraw-Hill, 1967..
28. Weinberg, H. : Application of Ray Theory to Acoustic Propagation in Horizontally Stratified Oceans. J. Acoust. Soc. Am., Vol. 58, No. 1, 1975. pp 97-109
29. Wilson, W.D. : Speed of Sound in Sea Water as a Function of Temperature, Pressure and Salinity. J. Acoust. Soc. Am., Vol. 32, 1960. pp 1357
30. Witner, D.R. and Pearson, R.E. : Acoustic Telemetry - an Underwater Alternative. 9th Annual Offshore Technology Conference, Texas, 1977. pp 461-466

31. Witner, D.R. and Pearson, R.E. : Acoustic Telemetry
- a Step Toward an Underwater Alternative. J. Petr.
Tech., Oct. 1978. pp 1403-1406
32. Zielinski, A. and Barbour R. : The Swept Carrier
Underwater Acoustic Communication System. 5th Inter-
national Ocean Development Conf., Tokyo, Japan,
Sept. 1978. pp F2/1-16
33. Zielinski, A. and Barbour R. : Swept Carrier
Acoustic Underwater Communications. IEEE Marine. Tech.
Soc., Sept. 1978. pp 60-65

APPENDIX A

Time Spread due to Frequency-dependent Absorption

A wave propagating through the ocean is subjected to a frequency-dependent attenuation due to absorption. The amplitude response for any range can be calculated based on the absorption coefficient as:

$$|H(f)| = \left[\frac{-df^2}{914} \cdot \frac{.1}{1+f^2} + \frac{40}{4100 + f^2} + 2.75 \times 10^{-4} \right] \quad (A.1)$$

where: $|H(f)|$ = amplitude response of the ocean transfer function in dB

d = path travel distance in m

f = frequency in kHz

Since the speed of sound in water is constant to within 1% [6], the travel times for all frequencies is nearly constant. The ocean's transfer function therefore is assumed to have a linear phase characteristic:

$$\phi(f) = -2\pi ft_o \quad (A.2)$$

where: $\phi(f)$ = the ocean transfer function phase response

t_o = travel time along distance d in s

Knowing the amplitude and phase responses, the inverse Fourier transform produces the impulse response for the ocean at a distance d .

The ocean transfer function can be modelled, as in Figure A.1, by a filter having the amplitude response equal to $|H(f)|$, in series with an all-pass filter with a time delay of t_d . The transfer function with a lms delay has been programmed on the Fourier Analyser to perform the inverse Fourier transform. This show that the impulse response of the ocean is a pulse with a range-dependent spread. Figures A.2 a,b,c show the time spread associated with ranges of 500m, 1000m and 5000m respectively. These figures show that the time spread (measured at 50% of the peak value) caused by the ocean's amplitude response ranges from 25 μs for 500m to 60 μs for 5000m.

This effect, however, is very small compared to the time smear due to the multipath and has therefore been neglected in the eigenray response program.

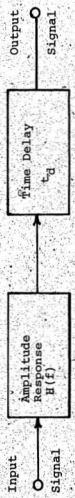


Figure A.1 Block Diagram of Ocean Transfer Function

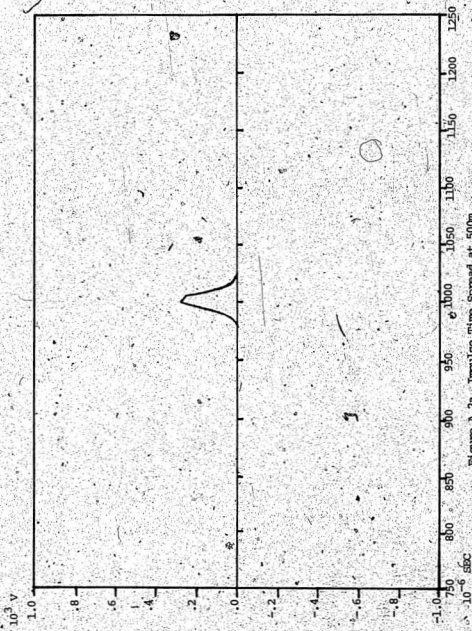


Figure A.2a Impulse Time Spread at 500m

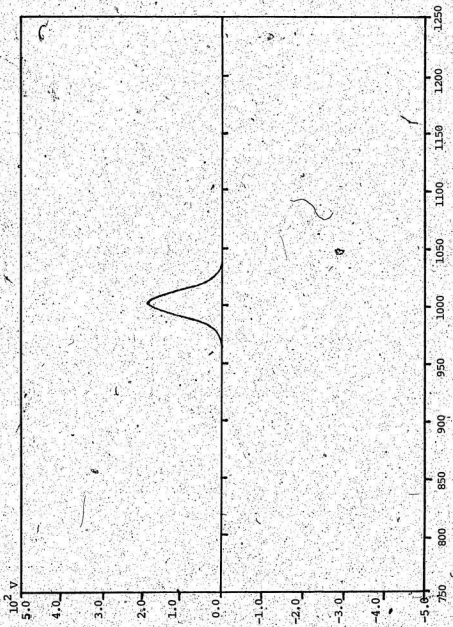


Figure A.2b Impulse Time Spread at 1000m

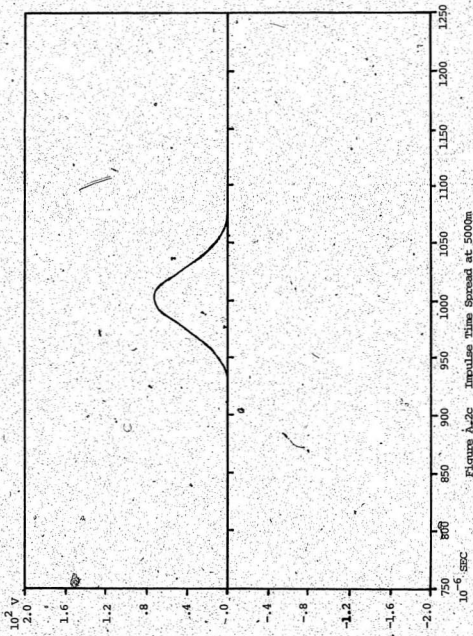


Figure A.2c Impulse Time Spread at 5000m

APPENDICE B

RAY-TRACE PROGRAM

Ray Trace Program Listing

```

0: "RAY TRACE
PROGRAM":
1: emp "    DATA
FILE      LOCA
TION (M)",M
2: dim A$[10]
3: emp "NO. OF
DEPTH INCREMENT
S (F)",F
4: emp "MAX.
HORIZONTAL DIST
ANCE H(m)",H
5: emp "MAX.
DEPTH X(m)",X
6: emp "MAX.
RAY ABOVE HORI
Z. P(degrees)",P
7: emp "MAX.
RAY BELOW HORI
Z. B(degrees)",B
8: emp "DELTA
ANGLE      D(de
grees)",D
9: emp "SOURCE
DEPTH Y(m)",Y
10: emp "DISCRET
E ANGLES?",AS
11: if cap(A$[1,
1])#Y" and
cap(A$[1,1])#N
";jmp-1
12: trk 1
13: dim C[1:50],
D[1:50],Z[1:F+
1],V[1:F+1],.
G[1:F+1],A[1:(P-
B)/D+1]
14: dim M[1:(P-
B)/D+1],T[1:(P-
B)/D+1],U[1:(P-
B)/D+1]
15: ldf M,C[*],
D[*]
16: trk 0
17: scl -.16,
.152,-.12,.16
18: plt -.16,
.16;pen;plt
.152,.16;pen;
plt 1.52,-.12;
pen;plt -.16,-
1.12.
19: pen
20: plt 0,0;plt
1,0;plt 1,-1;
plt 0,-1;plt 0,
0
21: pen
22: plt 1.04,0;
plt 1.44,0;plt
1.44,-1;plt
1.04,-1;plt
1.04,0
23: pen
24: plt 0,0
25: pen
26: .2-T"
27: gsb "ticX"
28: plt 1,0
29: pen
30: -.2-T"
31: gsb "ticY"
32: plt 1,-1
33: pen
34: gsb "ticX"
35: plt 0,-1
36: pen
37: .2-T"
38: gsb "ticY"
39: plt 0,0
40: pen
41: plt 1.04,0
42: pen
43: .08+T
44: gsb "ticX"
45: plt 1.44,0
46: pen
47: -.2-T"
48: gsb "ticY"
49: plt 1.44,-1
50: pen
51: -.08+T
52: gsb "ticX"
53: plt 1.04,-1
54: pen
55: .2-T"
56: gsb "ticY"
57: plt 1.04,0
58: pen
59: gto 74
60: "ticX":for
I=1 to 4
61: iplt T,.01
62: iplt 0,-.02
63: iplt 0,.01
64: pen
65: next I
66: ret
67: "ticY":for
I=1 to 4
68: iplt .01,T
69: iplt -.02,0
70: iplt .01,0
71: pen
72: next I
73: ret
74: csiz 1,1,1,0
75: plt 0,-.08
76: if cap(A$[1,
1])#Y";lbl
"DISCRETE ANGLE
S";jmp 4
77: lbl "MAX.
ANGLE",b,
INC_ANGLE",D
78: plt 0,.04
79: lbl "MIN
ANGLE",B
80: plt -.1,-.7
81: csiz 1,1,1,
90
82: lbl "SOURCE
DEPTH",Y,"M"
83: csiz 1,1,1,0
84: cplt 45, #38;
fd 0
85: lbl "IN 1-
",M;fd 1,2
86: plt -.16,0
87: lbl "0.00M"
88: plt -.14,-
1.04
89: lbl X,"M";
cplt -5,-2;lbl
"0.00M";cplt
26,0;lbl H,"M"
90: X/F+r0
91: 0+r3;+r1
92: 1-N
93: (D[N+1]-D[N]
)/(C[N+1]-C[N])
+r1
94: "sta":I+1+I;
if I>F+1;gto
105
95: if r3>max(D[
*]);.016+r1;
r1+G[I];VII-1]+
r0*.016+V[I];
r3+Z[I];c3+r0+r3

```

```

96: if r3>max(D[ *]);gto "sta"
97: if r3=D[N]; D[N]+z[I];c[N]+V[I];r3+r0+r3;
1/r1-G[I];N+1->N;gto "sta"
98: if r3=0;if r3*D[N];C[N]-D[N]/r1+V[I];
r3-Z[I];1/r1-G[I];r3+r0+r3;gto "sta"
99: if r3>D[N];
if r3-r0<D[N];(D[N]-D[N])/C[N+1]-C[N])>x,
1;N+1-N
100: if r3>D[N];
if r3-r0<D[N];C[N]-(D[N]-r3)/r0+V[I];r3+Z[I];
r3+r0+r3
101: if r3>D[N];
if r3-r0<D[N];(V[I]-V[I-1])/r0+G[I];gto "sta"
102: if r3<D[N];
(D[N]-D[N-1])/C[N]-C[N-1])>x
1
103: if r3<D[N];
C[N]-(D[N]-r3)/r1-V[I];r3+Z[I];
r3+r0+r3;1/r1-G[I]
104: gto "sta"
105: l+I;P*D+E;
l-W
106: "start": if cap(A$[1,1])=="Y";
"emp" "NEW ANGL E? 90 to stop",
E;B+D+E;
107: 0-S;E-D+E;
E+B;0>L;0-K;
l+I;0-U;0+r4;
0+r5;pen;plt,0,-Y/X
108: if P=90;
gto "end"
109: if P<B;gto "end"
110: if Y=Z[I];
if P<0;Y-K;gto "neg"
111: if Y=Z[I];
if P>0;Y+K;gto "pos"
112: if Y=Z[I];
if P=0;Y-K;gto 122
113: if Z[I]>Y;
if P>0;(Y-Z[I-1])/abs(tan(P));
+S;iplt abs(S)/H,(Y-Z[I-1])/X
114: if Z[I]>Y;
if P<0;/(S+2+(-Z[I-1]))+2+r4;
4;r5+r4/V[I-1]+r5;Z[I-1]-K;
r4+L*L
115: if Z[I]>Y;
if P>0;I-1+I;
gto "pos"
116: if Z[I]>Y;
if P<0;/(S+2+(-Z[I-1]))+2+r4;
S;iplt S/H,(Y-Z[I])/X
117: if Z[I]>Y;
if P<0;/(S+2+(-Z[I-1]))+2+r4;
Z[I]*K;r5+r4/V[I-1]+r5;Z[I]+K
118: if Z[I]>Y;
if P<0;r4+L*L;
gto "neg"
119: if Z[I]>Y;
if P=0;Y-K;gto 122
120: I+l+I
121: if I<=F+1;
gto 109
122: P+.0000001+P
123: "pos":if V[I-1]/V[I]*cos(P)>1;gto "bend"
124: if I=2;gto "surf"
125: abs(cos(P))>V[I-1]/V[I]*Q
126: r0/tan((P+Q)/2-J);Q+P
127: if S+J<H;
/(J+2+r0+2)*r4;
r4+L*L;K+r0*K;
r5+r4/V[I-1]+r5
128: if S+J>H;
iplt (H-S)/H,(-(H-S)tan(P))/X;
P+A[W]
129: if S+J>H;
/(H-S)+2+((H-S)tan(P))+2+r4
;r4+L*T[W]
130: if S+J>H;K-(H-S)tan(P)-M[W]
J;5+r4/V[I-1]+U[W];W+H*W;
gto "start"
131: S+J+S
132: iplt J/H,r0/X
133: if P>0;I-1+I;gto "pos"
134: if P=0;gto 122
135: "neg":if V[I]/V[I-1]*cos(P)>1;gto "bend"
136: if I=F;gto "pot"
137: abs(cos(P))V[I]/V[I-1]-Q
138: r0/abs(tan((P-Q)/2))+J;-Q
>P
139: if S+J<=H;
/(J+2+r0+2)*r4;
r4+L*L;K+r0*K;
r5+r4/V[I-1]+r5
140: if S+J>H;
iplt (H-S)/H,(-(H-S)abs(tan(P)))/X;P+A[W]
141: if S+J>H;
/(H-S)+2+((H-S)tan(P))+2+r4
;r4+L*T[W];K+M[W]

```

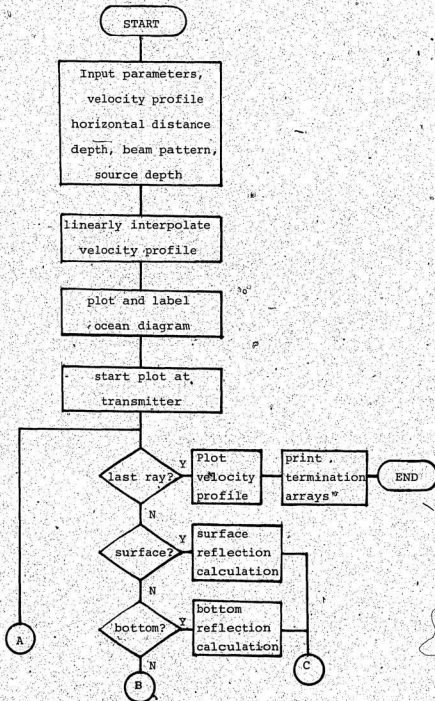
```

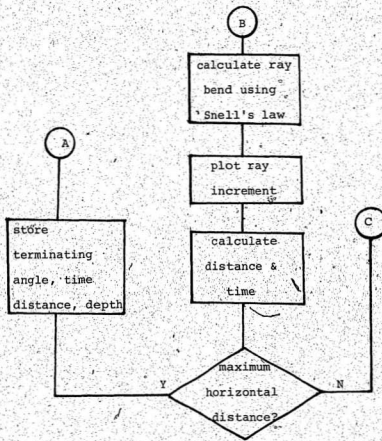
142: if S+J>H;
r5+r4/V[I+1]+U[1];
W];W+1-W;gto
"start"
143: S+J+S
144: iplt J/H,-r0/X
145: if P<0;I+1+I;gto "neg"
146: if P=0;gto
122
147: "bend":2V[I-1]/abs(G[I-1]*tan(P)+J
148: if S+J=H;
L+J-L;r5+r4/V[I-1]+r5
149: if S+J>H;
iplt (H-S)/H,0;
H-S+L+rT[W];P+A[W];
W];z5+(H-S)/V[I-1]+U[W];
K+M[W]
150: if S+J>H;W+1+W;gto "start"
151: S+J+S
152: -P+P
153: iplt J/H2,r0/X2;iplt J/H2,-r0/X2
154: gto "neg"
155: "bend":2V[I]/abs(G[I-1]*abs(tan(P))+J
156: if S+J>H;
L+J-L;r5+j/V[I]+r5
157: if S+J>H;
iplt (H-S)/H,0;
H-S+L+rT[W];P+A[W];
W];r5+(H-S)/V[I]+U[W];
K+M[W]
158: if S+J>H;W+1+W;gto "start"
159: S+J+S
160: -P+P
161: iplt J/H2,-r0/X2;iplt J/H2,+r0/X2
162: gto "pos"
163: "surf":acs(V[I-1]/V[I]*cos(P))-Q
164: r0/tan(Q)+J
165: S+2J<=H;
2/(J+2+r0+2)+r4
;r5+r4/V[I-1]+r5
5;r4+L-L'
166: -Q+P
167: if S+J>H;
iplt (H-S)/H,(H-S)tan(Q)/X;
/(H-S)+2+(H-S)tan(P))+2+r4
168: if S+J>H-K;
(H-S)tan(Q)+M[W]
169: if S+J>H;
r4+rT[W];P+A[W];
r5+r4/V[I-1]+U[W];W+1+W;
gto "start"
170: if S+2J>H;
iplt J/H,r0/X;
S+J-S;iplt (H-S)/H,tan(P)*(H-S)/X
171: if S+J>H;
/(J+2+r0+2)+
/(H-S)+2+(tan(P)-(H-S))+2+r4;
r4+rT[W]
172: if S+J>H;
(H-S)tan(Q)+M[W]
173: if S+J>H;
90-P+A[W];r5+r4/V[I-1]+U[W];
W+1+W;gto "star"
174: S+2J+S
175: iplt J/H,r0/X
176: iplt J/H,-r0/X
177: gto "neg"
178: "bot":acs(os(P)*V[I]/V[I-1])+Q
179: r0/abs(tan(Q))+J
180: if S+2J<=H;
2/(J+2+r0+2)+r4
;r5+r4/V[I]+r5
r4+L-L'
181: Q+P
182: if S+J>H;
iplt (H-S)/H,(-H+S)tan(Q)/X;
/(H-S)+2*((-H+S)tan(P))+2+r4
183: if S+J>H-K;
(H-S)tan(Q)+M[W]
184: if S+J>H;
r4+rT[W];P+A[W];
r5+r4/V[I]+U[W];W+1+W;gto
"start"
185: if S+2J>H;
iplt J/H,-r0/X;
S+J-S;iplt (H-S)/H,(H-S)tan(Q)/X
186: if S+2J>H;
/(J+2+r0+2)+
/(H-S)+2+(tan(P))+2+r4;
r4+rT[W]
187: if S+J>H-X;
(H-S)tan(P)+M[W]
188: if S+J>H;
90-P+A[W];r5+r4/V[I]+U[W];W+1+W;gto "start"
189: S+2J+S
190: iplt J/H,-r0/X
191: iplt J/H,r0/X
192: gto "pos"
193: "end":dsp
"RAY TRACE COMP
LETB";pen
194: plt 1.04,.12
195: lbl "Qmin
Cmax"
196: cplt -15,-2
197: lbl min(V[*]);
,"",max(V[*])
198: plt 1.04,.04
199: lbl "0.0%
100.0%",pen
200: for I=1 to
F+1

```

```
201: (V[I]-min(V
    [*]))/(max(V[*]
   ])-min(V[*]))*
    .4+1.04+r6
202: -(Z[I]-min(
    Z[*]))/(max(Z[*]
    )-min(Z[*]))+r
    7
203: plt r6,r7
204: next I
205: pen
206: dsp "END
    OF RAY TRACE"
207: for I=1 to
    N
208: (C[I]-min(V
    [*]))/(max(V[*]
    )-min(V[*]))*
    .4+1.04+r6
209: -(D[I]-min(
    Z[*]))/(max(Z[*]
    )-min(Z[*]))+r
    7
210: if r7<-1;
    plt 1.52-.16;
    pen;gto "arr"
211: plt r6,r7;
    cpt -.3,-.3;
    lbl "+";pen
212: next I
213: "arr":prt
    RAY DISTANCE
    ARRAY"
214: aptt T
215: prt "TERMIN
    ATING      ANGLE
    ARRAY"
216: aptt A
217: prt "PROPAG
    ATION TIME ARRA
    Y"
218: aptt U
219: prt "TERMIN
    ATING      DEPTH
    ARRAY"
220: aptt M
221: "end":dsp
    "END OF RAY
    TRACE PROGRAM";
    end
```

Figure B.1 Flowchart for Ray Trace Program





APPENDICE C

EIGENRAY RESPONSE PROGRAM

Eigenray Response Program Listing

```

0: "EIGENRAY
  RESPONSE PROGRA
M";
1: emp " DATA
FILE LOCATION
(M",M
2: emp "NO. OF
DEPTH INCREMENT
S (F),F
3: emp "MAX.
HORIZONTAL DIST
ANCE H (m)",H
4: emp "MAX.
DEPTH X (m),X
5: emp "MAX:
RAY ANGLE P(deg
rees)",P
6: emp "MIN.
RAY ANGLE B(deg
rees)",B
7: emp "DELTA
ANGLE D(de
gress)",D
8: emp "SURFACE
LOSS (dB)",rl4
9: emp "BOTTOM
LOSS (dB)",rl5
10: emp "SOURCE
DEPTH Y(m)",Y
11: psc 5
12: trk 1
13: dim A$[10],
Q[(P-B)/D+1,8]
14: dim C[1:50],
D[1:50],Z[1:F+
1],V[1:F+1],
G[(F+1)],A[1:(P-
B)/D+1]
15: dim M[1:(P-
B)/D+1],T[1:(P-
B)/D+1],U[1:(P-
B)/D+1]
16: emp "PRINT
TERMINATING
ARRAYS?",A$
17: emp "FREQUEN
CY (KHz)",r2
18: emp "RECEIVE
R DEPTH (M)",G
19: emp "DEPTH
TOLERANCE (M)",
r8
20: emp "MAX.
NO. OF ITERATIO
NS",r21
21: scl -.16,
1.52,-1.12,.16'
22: ldf M,C[*],
D[*]
23: trk 0
24: P+r9
25: B+r18
26: psc 0
27: gto "subs"
28: "ticX":for
I=1 to 4
29: iplt T,.01
30: iplt 0,-.02
31: iplt 0,.01
32: pen
33: next I
34: ret
35: "ticY":for
I= 1 to 4
36: iplt .01,T
37: iplt -.02,0
38: iplt 01,0
39: pen
40: next I
41: ret
42: "subs":gsb
"vel"
43: gsb "rays"
44: gto "arr"
45: "vel":X/F+r0
46: 0+r3;0+I
47: 1-N
48: (D[N+1]-D[N]
)/(C[N+1]-C[N])
+r1
49: "sta":I+l+1;
if I>F+1:gto 60
50: if r3>max(D[
]*);.016+r1;
r1+G[I];V[I-1]+
r0*.016+V[I];
r3+Z[I];r3+r0+r*
3
51: if r3>max(D[
]);gto "sta"
52: if r3=D[N];
D[N] Z[I];C[N]+
V[I];r3+r0+r3;
1/r1+G[I];N+
1-N:gto "sta"
53: if r3=0;if
r3#D[N]:C[N]-
D[N]/r1+V[I];
r3+Z[I];1/r1-G[
I];r3+r0+r3;
gto "sta"
54: if r3>D[N];
if r3-r0<D[N];
(D[N+1]-D[N])/
(C[N+1]-C[N])+r
1;N+1-N
55: if r3>Q[N];
if r3-r0<D[N];
C[N]-(D[N]-r3)/
r1+V[I];r3+Z[I]
;r3+r0+r3
56: if r3>D[N];
if r3-r0<D[N];
(V[I]-V[I-1])/
r0+G[I];gto
"sta"
57: if r3<D[N];
(D[N]-D[N-1])/
(C[N]-C[N-1])+r
1
58: if r3<D[N];
C[N]-(D[N]-r3)/
r1-V[I];r3+Z[I]
;r3+r0+r3;1/
r1-G[I]
59: gto "sta"
60: ret
61: "rays":l+I;
P+D+E;l+N
62: if T>0;0+Q[T
,8]
63: "start":0+S;
E-D+E;B+P;0+L;
64: disp "ANGLE",
E
65: if P<B:gto
"end"
66: if Y=Z[I];
if P<0;Y-K;gto
"neg"
67: if Y=Z[I];
if P>0;Y+K;gto
"pos"

```

```

68: if Y=Z[I];
if P=0;Y>K;gto
78
69: if Z[I]>Y;
if P<0;(Y-Z[I-1])/abs(tan(P))+S;iplt abs(S)/H,(Y-Z[I-1])/X
70: if Z[I]>Y;
if P 0;/(S+2*(Y-Z[I-1])+2)+r4;r5+r4/V[I-1]+r5;Z[I-1]+K
71: if Z[I]>Y;
if P<0;I-1-I;r4+L+L;gto "pos"
72: if Z[I]>Y;
if P<0;/(Z[I]-Y)/abs(tan(P))+S;iplt S/H,(Y-Z[I])/X
73: if Z[I]>Y;
if P<0;/(S+2*(Y-Z[I-1])+2)-r4;Z[I]-K;r5+r4/V[I-1]-r5;Z[I]+K
74: if Z[I]>Y;
if P<0;r4+L+L;gto "neg"
75: if Z[I]>Y;
if P=0;Y>K;gto
78
76: I+1+I
77: if I<=F+1;
gto 65
78: P+.00000001+P
79: "pos":if
V[I-1]/V[I]*cos(P)>1;gto "bend"
80: if I=2;gto "surf"
81: acs(cos(P)*V[I-1]/V[I])~Q
82: r0/tan((P+Q)/2)+J-Q+P
83: if S+J<=H;/(J+2+r0+2)+r4;r4+L+L;K+r0+K;r5+r4/V[I-1]+r5
84: if S+J>H;
iplt (H-S)/H,(H-S)tan(P)/X;P+A[W]
85: if S+J>H;
✓((H-S)+2+((H-S)tan(P))+2)+r4;r4+L+L;T[W]
86: if S+J>H-K-(H-S)tan(P)-M[W];J;r5+r4/V[I-1]+U[W];W+1+W;
gto "start"
87: S+J+S
88: iplt J/H,r0/X
89: if P>0;I-1+I;gto "pos"
90: if P=0;gto
78
91: "neg":if
V[I]/V[I-1]*cos(P)>=1;gto "bendn"
92: if I=F;gto "bot"
93: acs(cos(P)V[I-1]/V[I-1])~Q
94: r0/abs(tan((P-Q)/2))~J-Q+P
95: if S+J<=H;✓(J+2+r0+2)+r4;r4+L+L;K+r0+K;r5+r4/V[I-1]+r5
96: if S+J>H;
iplt (H-S)/H,-H+S;abs(tan(P))/X;P+A[W]
97: if S+J>H;
✓((H-S)+2+((H-S)tan(P))+2)+r4;r4+L+L;T[W];K+r0+K;r5+r4/V[I-1]+r5
98: if S+J>H;r5+r4/V[I-1]+U[W];W+1+W;gto "star"
99: S+J+S
100: iplt J/H,-r0/X
101: if P<0;I-1+I;gto "neg"
102: if P=0;gto
78
103: "bendp":2V[I-1]/abs(G[I-1])*tan(P)~J
104: if S+J<=H;L+r5;L;r5+J/V[I-1]+r5
105: if S+J>H;
iplt (H-S)/H;0;H-S+r5;T[W];P+A[W];r5+(H-S)/V[I-1]+U[W];K+M[W]
106: if S+J>H;W+1+W;gto "start"
107: S+J+S
108: -P+P
109: iplt J/H2,r0/X2;iplt J/H2,-r0/X2
110: gto "neg"
111: "bendn":2V[I]/abs(G[I+1])*abs(tan(P))~J
112: if S+J<=H;L+r5;L;r5+J/V[I]+r5
113: if S+J>H;
iplt (H-S)/H;0;H-S+r5;T[W];P+A[W];r5+(H-S)/V[I]+U[W];K+M[W]
114: if S+J>H;W+1+W;gto "start"
115: S+J+S
116: -P+P
117: iplt J/H2,-r0/X2;iplt J/H2,r0/X2
118: gto "pos"
119: "surf":acs(V[I-1]/V[I]*cos(P))~Q
120: r0/tan(Q)~J
121: if S+2J<=H;2/(J+2+r0+2)+r4;r5+r4/V[I-1]+r5;r4+L+L
122: -Q+P;if T<0;r14+Q*T,8+Q[T,8]

```

```

123: if S+J>H;
iplt -(H-S)/H,
(H-S)tan(Q)/X;
/((H-S)+2*((H-
S)tan(P))+2*x4
124: if S+J>H;K-
(H-S)tan(Q)+M[W
]
125: if S+J>H;
r4+L+T[W];P+A[W
];r5+r4/V[I-
1]+U[W];W+1+W;
gto "start"
126: if S+2J>H;
iplt J/H,r0/X;
S+J+S;iplt (H-
S)/H,tan(P)*[H-
S]/X
127: if S+J>H;
/(J+2+r0/2)+
/((H-S)+2+(tan(
P*(H-S))+2)+x4;
r4+L+T[W]
128: if S+J>H;
(H-S)tan(Q)+M[W
]
129: if S+J>H;
90-P+A[W];r5+
r4/V[I-1]+U[W];
W+1+W;gto "star
t"
130: S+2J+S
131: iplt J/H,
r0/X
132: iplt J/H,-
r0/X
133: gto "neg"
134: "bot":acs(c
os(P)*V[I]/V[I-
1])>Q
135: r0/abs(tan(
Q))>J
136: if S+2J<=H;
2/(J+2+r0/2)+x4
;r5+r4/V[I]+r5;
r4+L+L
137: Q+P;if T>0;
r15+Q[T,8]>Q[T,
8]
138: if S+J>H;
iplt (H-S)/H,(-
H+S)tan(Q)/X;
/((H-S)+2*((-H-
S)tan(P))+2*x4
139: if S+J>H;K+
(H-S)tan(Q)+M[W
]
140: if S+J>H;
r4+L+T[W];P+A[W
];W+1+W;gto
"start"
141: if S+2J>H;
iplt J/H,-r0/X;
S+J+S;iplt (H-
S)/H,(H-S)tan(Q
)/X
142: if S+J>H;
/(J+2+r0/2)+
/((H-S)tan(P))+
2*(H-S)+2)+x4;
r4+L+T[W]
143: if S+J>H;X-
(H-S)tan(P)+M[W
]
144: if S+J>H;
90-P+A[W];r5+
r4/V[I]+U[W];W+
1+W;gto "start"
145: S+2J+S
146: iplt J/H,-
r0/X
147: iplt J/H,
r0/X
148: gto "pos"
149;"end";if
r10=0;dsp "RAY
TRACE COMPLETE"
150: ret
151: "arr":if
cap(A$[1,1])="N
";gto "skip"
152: prt "RAY
DISTANCE
ARRAY"
153: aptx T
154: prt "TERMIN
ATING ANGLE
ARRAY"
155: aptx A
156: prt "PROPAG
ATION TIME ARR
AY"
157: aptx U
158: prt "TERMIN
ATING DEPTH
ARRAY"
159: aptx M
160: dsp "END
OF RAY TRACES
PROGRAM"
161: "skip":for
I=1 to (r9-B)/D
162: if M[I]<G;
if M[I+1]>G;
gto "cross"
163: if M[I]>G;
if M[I+1]<G;
gto "cross"
164: gto "next"
165: "cross":r10
+r1+r10
166: r9-D*(I-
1)+Q[r10,1];r9-
D*I+Q[r10,2]
167: M[I]=Q[r10,3]
;M[I+1]=Q[r10,4]
168: "next":next
I
169: for T=1 to
r10
170: dsp "MULTIP
ATH",T,"BEING
CALCULATED";
wait 3000
171: "intpol":if
r20-1>=r21;
prt "MULTIPATH"
,T,"DID NOT
CONVERGE"
172: if r20>=r21
;disp "NO CONVER
ENCE";0>r20;
wait 5000;gto
"more"
173: Q[T,1]-(Q-
Q[T,3])*Q[T,
1]-Q[T,2])/Q[T
,4]-Q[T,3])>P;
r20+1>r20
174: .001+D;P+B
175: gsb "rays"
176: if abs(G-
M[1])<abs(r8);
gto "store"
177: if abs(Q[T,
3]-M[1])<abs(Q[
T,3]-G);B+D*Q[T
,1];M[1]=Q[T,3
]
;gto "intpol"

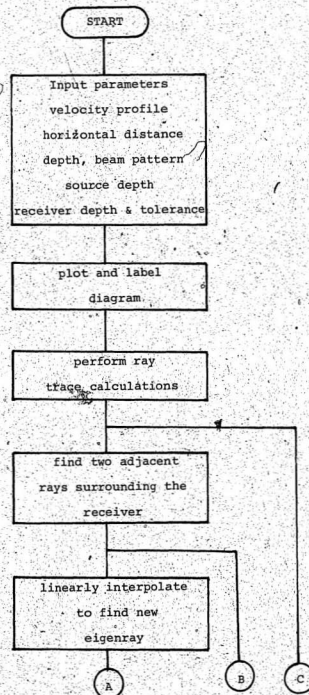
```

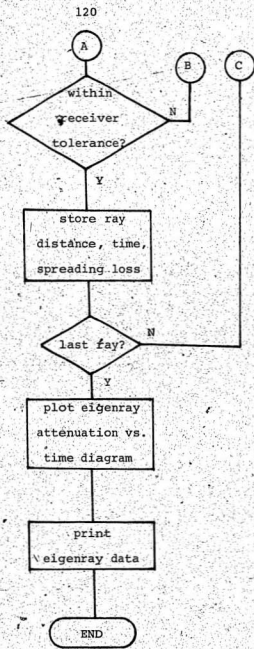
```

178: B+D*Q[T,2];
M[1]+Q[T,4];
gto "interp";
179: "store":B+Q
[T,1];M[1]+Q[T,3]
;U[1]-Q[T,5];
T[1]-Q[T,6];
A[1]-Q[T,7];
0+r20;
180: P-D:P+P+B
181: gsb "rays"
182: B+Q[T,2];
abs[M[1]-Q[T,3]
])>Q[T,4]
183: "more":next
T
184: dsp "ATTENU
ATION-BEING
CALCULATED"
185: 1.0936e-
3(1.^r2+2/(1+
r2+2)+40*r2+2/(-
4100+r2+2)+
2.75e-4*r2+2)+r
13
186: for T=1 to
r10
187: 1.19596*H*
-Q[T,4]*V[prnd(G
*x/X,0)]*180/
(D*V[prnd(Y*F/
X,0)])*n+r12
188: r13*Q[T,6]+
10*log(r12)+
Q[T,8]+Q[T,8]
189: next T
190: psc 5
191: scl -16,
1.16.-1.12,.16
192: plt -.16,
.16;pen/plt
1.16;.16;pen;
plt 1.16,-1.12;
pen;plt -.16,
1.12;pen
193: plt 0,0;
plt 1,0;plt 1,-
1;plt 0,-1;plt
0,0;pen
194: .2*T
195: gsb "ticx"
196: plt 1,0;pen
197: -.2*T
198: gsb "ticr"
199: plt 1,-1;
pen
200: gsb "tict"
201: plt 0,-1;
pen
202: .2*T
203: gsb "ticy"
204: plt 0,0;pen
205: csiz 1,1,1,
0
206: plt 0,.12;
tbl "MAX. ANGLE
",r9,".DEG."
207: plt .55,
.1;tbl "MIN.
ANGLE",r18,".
DEG."
208: plt 0,.08;
tbl "SOURCE
DEPTH",Y," M"
209: plt .55,
.08;tbl "FREQUE
NCY",r2," KHz"
210: plt 0,.04;
tbl "RECEIVER
DEPTH",G," M"
211: plt .55,
.04;tbl "TOLER
ANCE",r8," M"
212: csiz 1.5,1,
1.90
213: plt -.05,-
.75
214: lbl "ATTENU
ATION (dB)"
215: csiz 1,1,1,
0
216: fxd 1
217: plt -.16,0-
.16;pen
218: r10+T
219: dim K[T]
220: for I=1 to
r10
221: Q[I,8]+K[I]
222: next I
223: .1*int(10*
min(K[*]))+r1
4
224: lbl r14
225: plt -.16,-1
.16;pen
226: .1+.1*int(1
0*max(K[*]))+r
5
227: lbl r15
228: fxd 2
229: for I=1 to
r10
230: Q[I,5]-K[I]
231: next I
232: .1*int(10*
min(K[*]))+r16
233: plt -.08,-
1.04
234: lbl r16
235: .1+.1*int(1
0*max(K[*]))+r1
7
236: plt .95,-
1.04
237: lbl r17
238: plt .35,-
1.08
239: csiz 1.5,1,
1.0
240: lbl "TIME
(SEC)"
241: csiz 1,1,1,
0
242: plt 0,0;pen
243: for I=1 to
r10
244: plt (Q[I,
5]-r16)/(r17-
r16),-1
245: iplt 0,(Q[I
,8]-r15)/(r14-
r15)
246: cplt -.3,-
.3
247: lbl "X";pen
248: next I
249: fnt f5.1,
f5.2,f6.1
250: prt "ANG.
TIME ATN."
prt
251: prt " Deg.
Sec. dB";prt
252: for I=1 to
r10
253: wrt 16,Q[I,1]
,Q[I,5],Q[I,8]
254: next I
255: dsp "MULTIP
ATH COMPLETE"
256: "stop":end

```

Figure C.1 Flowchart for Eigenray Response Program





APPENDICE D

SCHEMATIC DIAGRAMS

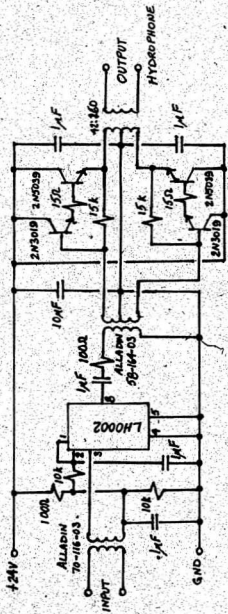


Figure D.1a Ametek Power Amplifier Schematic

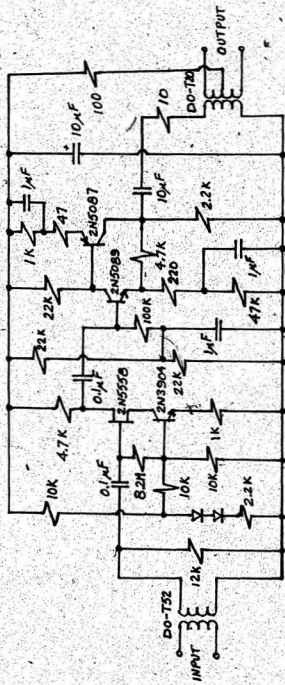


Figure D1b. AMETEK Preamp Schematic

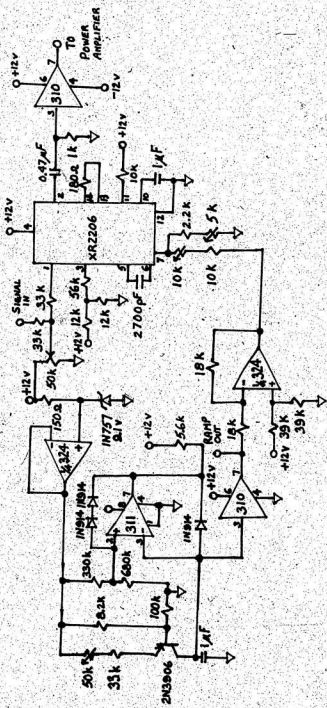


Figure D.1c Swept-Carrier Board Schematic

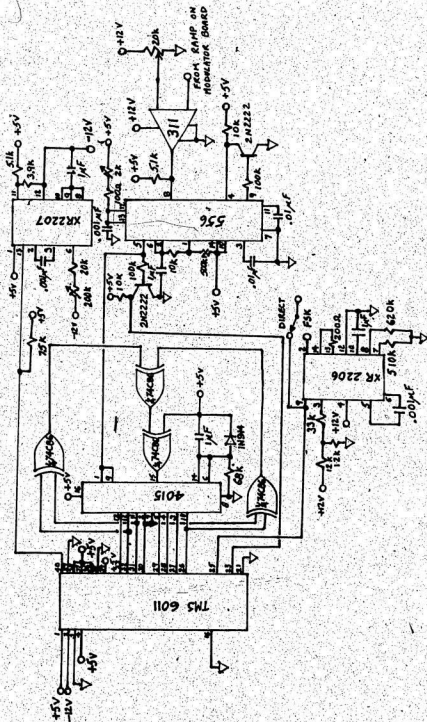


Figure D.1d Data Generator Board Schematic

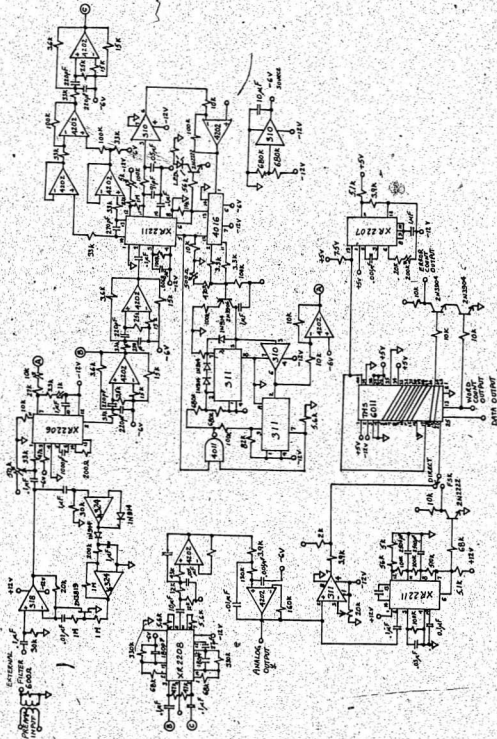


Figure D.1e Receiver Schematic

APPENDICE E

TRANSDUCER FREQUENCY RESPONSE

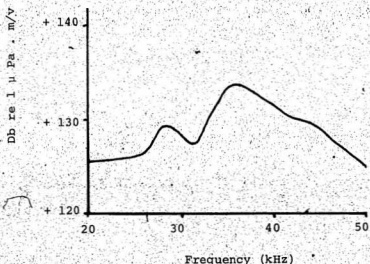


Figure E.1 Transducer transmitting response

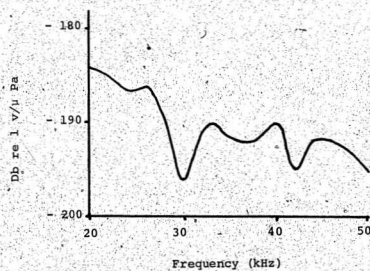


Figure E.2 Measured transducer receiving response

